# Journal of Materials Chemistry A

**REVIEW**

# Nanostructured Anode Materials for Lithium Ion Batteries

Poulomi Roy*[a] and Suneel Kumar Srivastava*[b]

The high-energy consumption in our day-to-day life can be balanced not only by harvesting pollution-free renewable energy sources, but also requires proper storage and distribution of energy. In this regard, lithium ion battery is currently considered as an effective energy storage device and involved most active research. There exist several review articles dealing with various sections of LIB, such as anode, cathode, electrolytes, electrode-electrolyte interface etc. However, anode is considered to be a crucial component effecting the performance of LIB as evident from the tremendous amount of current research work carried out in this area. In last few years, advancements are focused more on the fabrication of nanostructured anode owing to special properties, such as, high surface area, short Li$^+$ ion diffusion path length, high electron transportation rate etc. As the work in this area is growing very fast, the present review paper deliberates the recent developments of anode materials in the nanoscale dimensions. Different types of anode materials, such as, carbon-based material, alloys, Si-based materials, transition metal oxides, and transition metal chalcogenides with their unique physical and electrochemical properties are discussed. Various approaches on designing materials in the form of 0, 1 and 2D nanostructures and their effect of size and morphology on the performance as anode material in LIB are reviewed. Moreover, the article emphasizes the smart approaches of making core-shell, nanoheterostructures, nanocomposites or nanohybrids with the combination of electrochemically active materials and conductive carbonaceous or electrochemically inactive material to achieve LIBs with high capacity, high rate capability, and excellent cycling stability. We believe the review paper will provide an updated scenario to the reader about recent progress on the nanostructured anode material of LIB.

## 1. Introduction

The steady increase in energy consumption in many sectors is direct reflection of the economic growth of a country. However, this field became challenging due to unsustainable nature of non-renewable energy resources and to control $CO_2$ emission associated with global warming. Therefore, alternative environmentally friendly renewable sources, such as, solar cell, wind energy, hydropower etc. have been extensively explored. Concurrently, technology for storing energy as well as a proper distribution of energy is highly required due to unpredictable nature of renewable electricity sources. Therefore, a considerable amount of research has been focused in recent years on the development of materials for their applications in energy storage devices.

[a]Department of Chemistry, Birla Institute of Technology Mesra, Ranchi 835215, Jharkhand, India.
Email: poulomiroy@yahoo.com
[b]Department of Chemistry, Indian Institute of Technology Kharagpur, Kharagpur 721302, West Bengal, India.
Email: sunit@chem.iitkgp.ernet.in;
Fax: 0091-3222-28303; Tel: 0091-3222-283334

In this regard, battery and the electrochemical capacitor both can act as a portable or stationary store of electric power. Accordingly, technologies have been developed for nickel-cadmium, nickel–metal hydride, lead acid, lithium ion battery etc.[1, 2] In this context, rechargeable lithium ion battery (LIB) with high charge/discharge current rates were found to be very promising since first commercial launch by Sony[3] for their application in different portable electronic devices. The development have been extended to next generation energy storage devices with high power and high energy density for using in large scale application with electric and hybrid electric vehicles (EVs and HEVs).[4-6] The US company, General Motors first released the electric car EV-1 in 1996, based on lead acid battery.[7] However, due to the low energy density of lead acid battery, the second generation EV was released on 1999 based on nickel hydride battery. The possibilities of permanent damage of nickel hybrid battery on complete discharging limits the extensive use in EVs. After successful application in portable electronic devices, LIBs were also utilized in making EVs in order to get high-power and high energy density. Though due to toxic nature of cobalt-containing cathodes and

other safety issues, LIB-based EVs are still under development.[7] A HEV market evolution in Fig. 1 shows a steady increase in use of HEV worldwide since 2005 as reported by Scrosati et al.,[8] which clearly indicates a fast shifting towards technological innovation.

Though as per the current status performance wise EVs are not superior but equal to gasoline cars, in terms of fuel economy, availability of fuel/oils and most importantly as a clean energy it solves the problem of global warming protecting earth [7]. Therefore, large amount of funds have been invested in R&Ds to promote the development of LIB in several countries, like, United States, Europe and Japan.[8]
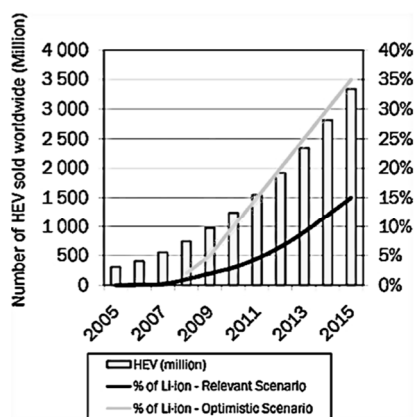


**Fig. 1**: HEV market evaluation. Reprinted with permission from ref 8. Copyright 2010 Elsevier.

In compared to other conventional batteries, LIB is light weight, more compact and works with an operating voltage of ~ 4 V and delivers with a specific energy ranging between 100 $WhKg^{-1}$ and 150 $WhKg^{-1}$ and capacity ranging from 700 to 2400 mAh for a single cell (battery).[9] A comparative plots of cell voltage vs. % of capacity discharged of different conventional batteries is shown in Fig. 2.[10]

In order to achieve high performance rechargeable LIB, several research works have been carried out. A very rapid growth in the exploration of various sections of LIB can be noticed from the plot of year-wise publication numbers, presented in Fig. 3. This shows the importance and inevitable usefulness of the field. The present review paper will mainly focus on the nanostructured anodes in the lithium ion battery and will survey use of different materials, nanoscale design of anode and their effect on the performance of LIB. The review paper not only discusses the success of using nanoscale anode material but the limitations encountered are also highlighted.
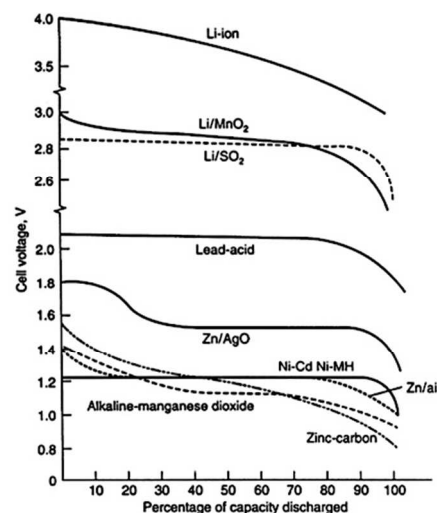


**Fig. 2**: A comparative study of battery discharge curves showing the variation of operating voltage vs. fraction of available capacity. Reprinted with permission from ref 10. Copyright 2009 Springer.
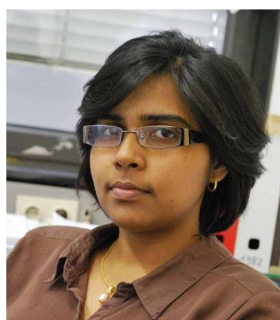
**Poulomi Roy** received her M.Sc. degree in Chemistry from Vidyasagar University, India in 2002 and obtained her PhD on Inorganic Nanomaterials from Indian Institute of Technology Kharagpur, India in 2007. She spent 2008-2011 at Friedrich-Alexander-Universität Erlangen-Nürnberg, Germany as a postdoctoral research fellow, where she worked on the development of self-organized $TiO_2$-based nanostructures and their various applications. Currently, she is working as an Assistant Professor at Birla Institute of Technology Mesra, India. Her current research interests include the synthesis of semiconductor nanomaterials and their applications in energy conversion and storage devices.

**Suneel Kumar Srivastava** was born in 1954 in Ismilepur (Sitapur), Uttar Pradesh. He received his M.Sc. degree in Inorganic Chemistry from Lucknow University, Lucknow. Subsequently, he completed his post graduate diploma in 'High pressure technology and technical gas reactions' and Ph.D in the field of 'Solid state chemistry' from Indian Institute of Technology, Kharagpur in 1979 and 1986, respectively. He also carried out his post-doctoral work as a DAAD Fellow in Technical University, Karlsruhe (1988–89, 2003, 2006), University of Siegen (1994, 1999), Technical University, Munchen (2009) and Leibniz Institute of Polymer Research, Dresden (2013) Germany, and University of Nantes, France (2003, 2007). He is currently Professor in the Department of Chemistry, Indian Institute of Technology, Kharagpur. His research interests are in the field zero, one and two dimensional semiconducting and magnetic nanomaterials for their application in energy and environments, polymer and polymer blends and their structure-property relationships. He has guided 12 Ph.D and published about 120 research papers in referred journals.

This journal is © The Royal Society of Chemistry 2014

*J. Mater. Chem.* A, 2014, **00**, 1-3 | **2**

Initially, it describes the classical electrochemistry of LIB mentioning the thermodynamic as well as kinetic aspects of ion transportation phenomena during lithiation-delithiation process. Further, the advantages of using nanostructured anode materials (carbonaceous, transition metal oxides, layered type transition metal dichalcogenides) in LIB battery have been highlighted. Also, recent progress in designing complex nanoheterostructures, nanocomposites, hybrid materials with proper combinations has been reviewed.
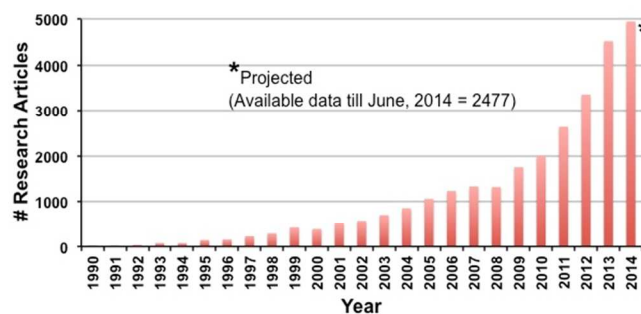


**Fig. 3**: A plot of year-wise publication number obtained by searching with keywords 'Lithium Ion Battery' (data source: www.scopus.com).

## 2. Electrochemistry of Lithium Ion Battery

A lithium ion battery consists of three major components: anode, cathode and an electrolyte and works by converting chemical energy into electrical energy. The choice of electrodes depends upon their electrochemical potential values ($\mu_A$ for anode and $\mu_C$ for cathode) as well as their positions to the HOMO-LUMO energy gap ($E_g$) of electrolyte. For a stable cell, $\mu_A$ must be lower in energy than the LUMO of electrolyte, otherwise the electrolyte will be reduced and on the other hand $\mu_C$ position should be in higher energy than HOMO of electrolyte to inhibit the oxidation of electrolyte as shown in Fig. 4a.[11] The high-energy storage density can be achieved in a cell with maximum electrochemical potential difference of anode and cathode as well as their high lithium intercalation ability though at the same time the stability of electrolyte should not be overlooked.[12]

In a conventional first generation LIB, graphite is used as anode and cathode is usually made of layered $LiCoO_2$ as intercalation host for $Li^+$, separated by a porous permeable membrane, which only allows $Li^+$ ions but prevents short circuit due to direct contact of electrodes. On charging the $Li^+$–ion de-intercalates from Lithium metal oxides (e.g., $LiCoO_2$) and passes through the Li-ion conductive electrolyte and intercalate to the layered graphite. A schematic diagram represented in Fig. 4b describes the mechanism in LIB. The lithium ion and electron generation occurs through following reactions:

*Cathode*: $LiCoO_2 \leftrightarrow Li_xCoO_2 + xLi^+ + xe^-$      (1)
*Anode*:   $6C + xLi^+ + xe^- \leftrightarrow Li_xC_6$          (2)
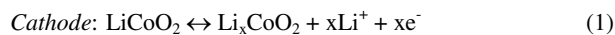
The electrons travel through the external electrical circuit in order to couple with the extra positive charge ($Li^+$) in the electrode. In discharging process, the reverse mechanism occurs. Selection of suitable electrolyte for a pair of electrodes in LIB is another important aspect. Mostly aprotic organic solvents mixed with Li-salts are commonly used as electrolytes

in LIB, e.g., alkyl carbonates (ethylene carbonate (EC), propylene carbonates (PC), diethyl carbonate (DEC)) mixed with lithium salts hexafluorophosphate ($LiPF_6$) or lithium perchlorate ($LiClO_4$).[13] Other than the energy gap of solvents, parameters, like, viscosity, dielectric constants to dissolve the solutes completely plays very important role in order to get a stable rechargeable cell.
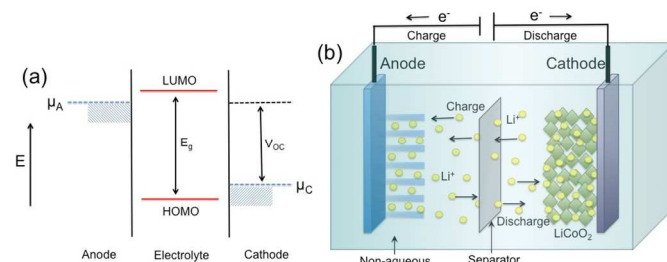


**Fig. 4**: (a) Relative energy diagram of electrode potentials and electrolyte energy gap in LIB; (b) Schematic diagram of lithium intercalation/de-intercalation reaction mechanism in rechargeable lithium-ion battery containing solid electrodes and liquid electrolyte.

The cell capacity is referred by the total charge transferred in the electrode-electrolyte interface, which depends on the current passed through the external circuit during charging-discharging process. At high current, during rapid charging the rate of ion transfer across electrode-electrolyte interfaces occurs in a diffusion-controlled mechanism.[14] It is predicted that Li may accumulate on the negative electrode and electrolyte interface when the Li-ion flux during the charge transfer reaction becomes higher than the Li-ion diffusion flux into the negative electrode.[15, 16] The massive dendritic growth of Li can be observed when the lithium ion concentration exceeds a certain saturation level (0.077 mol cm$^{-3}$). Such deposition leads to the deformation of underneath electrode surface, and causes internal short and thermal runway of battery.[15] Moreover, the dead Li deposited on the electrode surface creates internal resistance in cell and the changes at the electrode surfaces alters the rate due to slow diffusion of $Li^+$–ion at the interface resulting irreversible capacity fading. The electrochemical decomposition of electrolyte at the electrode-electrolyte interface is also responsible for capacity fading forming the solid-electrolyte interphase (SEI) layer on the active material. Though the SEI layer leads to irreversible capacity fading in a cell, it also act as a protective layer against further decomposition of electrolyte at the electrode-electrolyte interface.[9, 10] The characteristic Coulombic efficiency associated with capacity fading can be calculated as the fraction of the electrical charge stored during charging that is recoverable during discharge after each cycles, $100 \times \frac{Q_{dis}}{Q_{ch}}$.

## 3. Advantages of Nanostructured Anode

The selection of materials intimately depends on their crystal structure, physical properties (specific capacity, electrical conductivity, mechanical stability etc.), chemical properties (intercalation, reversibility) and many other factors. Other than the structure and properties of materials, size and shape of materials matter effectively on the performance of LIB. The first generation anode materials were basically micrometer-sized particles where the Li intercalation/de-intercalation

reactions occur. The rate of intercalation-deintercalation of lithium ion strongly depends upon the diffusivity of lithium ion.[17] The Li ion diffusion in a host material is associated with Li-ion diffusion coefficient and diffusion length in the material. In an indirect way diffusivity or diffusion length is represented as:

$$\tau = L_{ion}^{2} / D_{Li}$$

where, $L_{ion}$ is diffusion length and $D_{Li}$ is the diffusion coefficient.[18] While $D_{Li}$ depends upon the nature of material, $L_{ion}$ depends upon the size of material. Thereby the strategy to achieve high energy and high power or fast Li intercalation-deintercalation up to certain extends depends on controlling the size of materials. For example, rutile $TiO_2$ having low diffusion coefficient of $10^{-15}$ $cm^2/s$ are believed to accommodate a negligible amount of Li ions at room temperature.[6] However, significant changes can be observed for 5-15 nm sized rutile $TiO_2$ nanoparticles showing a full loading of lithium ($x > 1$ in $Li_xTiO_2$) and about 0.7 Li per rutile $TiO_2$ insertion-removal in subsequent cycles.[6, 19] Miniaturization of electrode materials also allows a large surface area in contact with the electrolyte resulting higher charge/discharge rates.[20-22] However, reduction of material size has not found to be always beneficial for the purpose. The very fast $Li^+$ intercalation-deintercalation often leads to undesirable side reactions and damage the battery life. Consequently, in last few years, nanomaterials in different morphology have been investigated for application as anodes in LIB.

**Nanoparticles**. Though nanostructured materials, especially the zero dimensional nanoparticles have been proven very effective in LIB, the performance is limited by various factors. For example, volume expansion and cracking of nanoparticles due to repeated $Li^+$ ion insertion and removal process during several cycles are major issue reducing the cyclability and thereby the battery life.[17] Both electron as well as $Li^+$ ion transportation through the nanoparticulate layers can be restricted due to random walk as shown in Fig. 5. Moreover, the grain boundaries, voids in between the nanoparticles limit the battery performances reducing electrical conductivity.[17, 20] Due to higher surface area of nanoparticles and access of electrolytes trigger the secondary reactions involving electrolyte decomposition and formation of solid electrolyte interphase (SEI) films at the interface between electrode and electrolyte. Though, formation of such SEI film in graphite anode inhibits the exfoliation, consumes excessive charge supplied by cathode exhibiting low coulombic efficiency and capacity loss.[17, 23] Several successful works on utilizing nanoparticles over micro/submicro particles are reported as anode material in LIB. Cheng et al.[24] studied the performances of NiO nanoparticles and sub-microparticles as anode in LIB and found that Nano-NiO was able to deliver more energy than SubM-NiO. Morphology-dependent performance of CuO anodes were also reported by Wang et al.[25] They prepared leaf-like CuO, oatmeal-like CuO, and hollow-spherical CuO nanostructures with controllable morphologies via solvothermal and calcination process. It was observed that leaf-like CuO and oatmeal-like CuO nanostructures exhibited decent electrochemical properties due to full penetration of electrolyte and availability of larger CuO-electrolyte contact area. However a decrease in reversible capacity values (563.8 to ~ 500 $mAhg^{-1}$ for leaf-like CuO and 637.7 to ~ 260 $mAhg^{-1}$ for oatmeal-like CuO after 55 cycles) during cycling was observed. In contrast, CuO hollowspheres showed an increase in reversible capacity (from 467.7 to 543.9 $mAhg^{-1}$ after 55 cycles) as the void space inside served as an effective elastic buffer to relieve the volume expansion during lithium-ion uptake/release and accommodate the strain in the CuO particles.

An approach to improvise the electron or ionic conductivity through the nanoparticulate films is the addition of conductive coating involving carbon or conductive polymer on nanoparticles.[26, 27] Such coating allows electrons or ions to travel through the conductive boundary of nanoparticles avoiding the interfacial resistance in between nanoparticles as shown in Fig. 5. Moreover, coating lead to stabilized SEI films on anodes, prevent direct contact of electroactive material with electrolytes and inhibit cracking, resulting in improved rate and cycling performance.[23] However, the addition of conductive binder leads to poor packing density of electrodes limiting the volumetric energy density.[23]
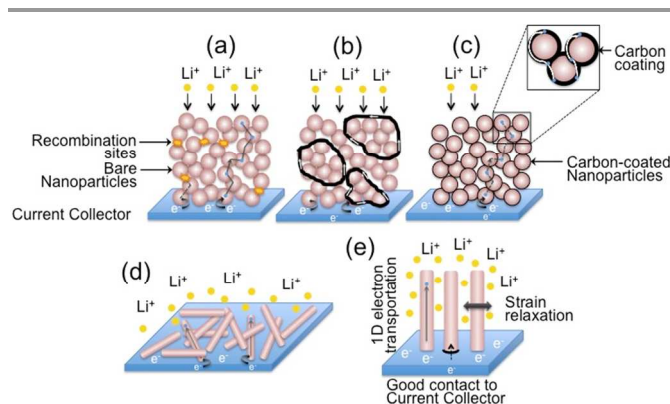


**Fig. 5**: Schematic diagram of electronic transportation through 0D, 1D nanostructures: (a-c) Electron random walk through grain boundaries of bare nanoparticles (a), through carbon binders blended with nanoparticles (b), and through carbon coating on to the nanoparticles (c); (d-e) 1D electron transportation through randomly distributed nanorods (d) and directly grown nanorods (e) on to the current collector.

Though graphite is known to be a good anode material in LIB, it has been coated with metallic Ni nanoparticles in order to further improve the electrical conductivity.[28-30] Such system not only shows an increase in exchange current densities and diffusion coefficients of the lithium ions, but also exerts decrease in the charge-transfer resistance and the surface film resistance in comparison with bare graphite, exhibiting less capacity loss over a 10-day storage period.[29] Other metals, such as, Cu, Ag, and Al can also be used as coating onto the graphite surface.[31-34] A small quantity of Co metal deposition on $SnO_2$ nanoparticles improved the performance of LIB significantly and exhibited an exceptional reversible capacity of 810 $mAhg^{-1}$ after 50 cycles.[35] Other than metal coating, coating with electronically conductive metal oxides, say $RuO_2$ coating on $TiO_2$ nanoparticles are also reported and found to have high capacity and extremely good power performance.[36] However, use of expensive $RuO_2$ coating on $TiO_2$ nanoparticles can be avoided by using graphene layer on nanostructured $TiO_2$.[37] Various reports are available on carbon coated $Li_4Ti_5O_{12}$ particles as anode material in order to attain high electrochemical performances.[38-41] Zhao et al.[39] fabricated N-doped carbon coated $Li_4Ti_5O_{12}$ particles using ionic liquid as the precursor of N-doped carbon simply by mixing $Li_4Ti_5O_{12}$ particles with ionic liquid followed by the pyrolysis of ionic liquid. The material showed a considerable improvement delivering a reversible capacity of 161 $mAhg^{-1}$, 145 $mAhg^{-1}$ and 129 $mAhg^{-1}$ at a current rate of 0.5C, 5C and 10C, respectively with very good capacity retention; while the uncoated sample only delivers 60 $mAhg^{-1}$ and 15 $mAhg^{-1}$ at a current rate of 5C and 10C, respectively.[26, 39] Nanosized Sn metal particles encapsulated within spherical hollow carbon is another very

interesting example as promising material to be used as anode in LIB exhibiting good cyclability preventing agglomeration of Sn nanoparticles and high volumetric energy density.[42, 43]

The conductive polymers, such as, polythiophene, polypyrrole and polyaniline have also been used as effective coating for nanoparticles.[44-46] Such polymer coating not only helps to improve the electrical conductivity, but prevent the direct contact of electrolyte with electroactive materials and minimize the SEI layer thickness and also proved to be very good binder due to their elasticity.[27] The polymer coating on the graphite surfaces found to be very promising as it effectively improves electrochemical performance of the composites in terms of the coulombic efficiency in the first cycle, the reversible capacity, the cycling behavior and the rate capability.[27]

**Nanorods, Nanotubes, Nanowires**. The disadvantages of using nanoparticles as anode in LIB, such as, loose contacts among nanoparticles and poor electronic or ionic transportation by random walk limiting the electron collection efficiency in the current collector can be addressed by using anisotropic nanostructures.[17, 20] One-dimensional nanostructures, such as, nanorods, nanowires, nanotubes are considered to be superior over nanoparticles due to directional electronic/ionic transportation leading to high electron collection efficiency. Moreover, the 1D structures also provide mechanical stability during several cycles of lithium insertion and removal process.[47] Therefore, several methods have been employed to fabricate 1D nanostructures, template assisted synthesis, hydrothermal method, electrodeposition or chemical vapor deposition techniques for their applications as anode in LIB.

The significant improvements in the battery performance are observed while anisotropic nanostructures are chosen over 0D

nanostructures. Cui and his co-workers developed an excellent anode electrode composed of Si nanowires.[47] The self-supported Si nanowires were grown directly onto stainless steel current collectors by vapour – liquid – solid growth method. The structural disintegration due to volume changes by 400% of bulk Si during Li ion insertion-removal cycles was successfully managed by this approach. An exceptionally high observed capacity value for Si NWs during the first cycle, 4277 mAhg$^{-1}$ decreased to 3541 mAhg$^{-1}$ at 2$^{nd}$ cycle and remained constant up to 10 cycles at C/20 rate. Though the initial irreversible loss in this case remained unexplainable, but the capacity stability after 2$^{nd}$ cycle was attributed due to accommodating strain and good contact between Si and current collector in such self-supporting nanostructure. The effect of anisotropic Si nanostructure was more noticeable from the comparative plot of capacity vs. cycle number of Si nanocrystals and Si NWs (Fig. 6a). The similar VLS mechanism was used to fabricate SnO$_2$ nanowires (dia: 40-50 nm, length: 1 μm) grown directly on the current collector.[48] The yielded nanowire arrays exhibited excellent stability in compared to SnO$_2$ and Sn nanopowders over 50 cycles. A much easier and cost-effective technique to fabricate self-supported metal oxides on to the current collector is ammonia-evaporation-induced method.[49, 50] Mesoporous Co$_3$O$_4$ NW arrays were directly grown on Ti foil by this technique and tested as the anode for LIB.[50] As expected, such self-supported arrangement showed excellent stability in reversible capacity after first charge/discharge process in the range of 700 mAhg$^{-1}$ at a current rate 1C up to 20 cycles. A comparative study with commercial Co$_3$O$_4$ powders and non-self-supported (broken) NWs mixed with carbon black and polymer binder under same electrochemical condition exhibit reversible capacity of 80 and 350 mAhg$^{-1}$, respectively up to 20 cycles along with sharp decay in capacity retention percentage (Fig. 6e).
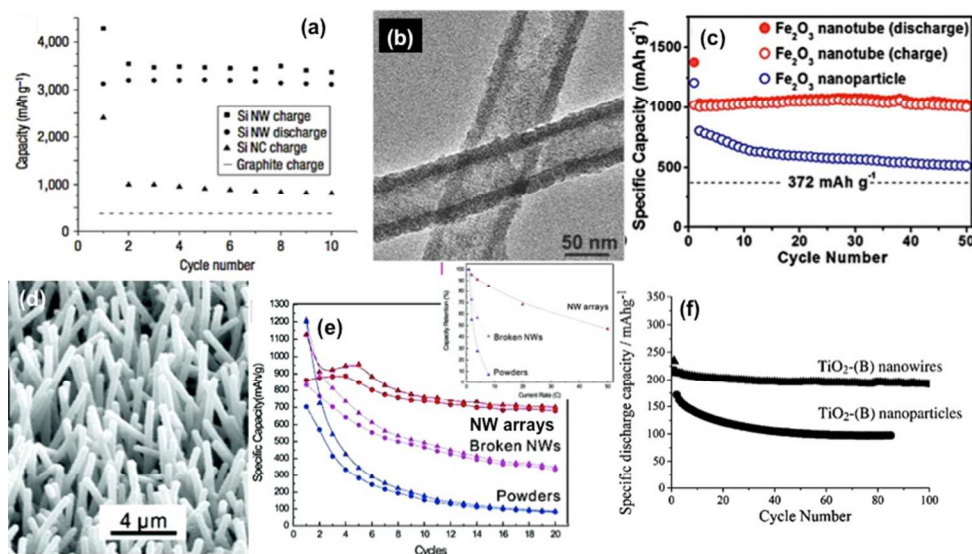


**Fig. 6**: 0D vs. 1D Nanostructures. (a) Capacity versus cycle number for the Si nanowires and Si nanocrystals at the C/20 rate. Reprinted with permission from ref 47. Copyright 2008 Nature Publishing Group. (b) TEM image of α-Fe$_2$O$_3$ nanotubes by template-engaged precipitation followed by annealing and (c) their cycling performance in comparison to α-Fe$_2$O$_3$ nanoparticles at 0.5 C (Ref. 56). (d) SEM images of Co$_3$O$_4$ NW arrays growing on Ti foil by ammonia-evaporation-induced method; (e) Comparative study of specific capacity of the Co$_3$O$_4$ NW arrays on Ti foil, non-self-supported NWs, and commercial powders as a function of the cycle number at a current rate 1C (*inset*: corresponding capacity retention percentages as a function of the current rate). Reprinted with permission from ref 50. Copyright 2008 American Chemical Society. (f) Comparison of lithium ion storage capacity of TiO$_2$ (B) nanowires and nanoparticles with same diameter. Reprinted with permission from ref 17. Copyright 2008 John Wiley and Sons.

The good cycleability and high rate capability of NW arrays is also considered to be due to porous nature of arrays allowing enhanced electrolyte/Co$_3$O$_4$ contact area, short the Li$^+$ ion diffusion length in the NWs, and accommodation of strain

induced by the volume change during the electrochemical reaction. The beneficial effect of 1D nanostructure is also observed for non-self supported materials. A considerable improvement in the electrode performance for TiO$_2$ (B)

This journal is © The Royal Society of Chemistry 2014

*J. Mater. Chem.* A, 2014, **00**, 1-3 | **5**

nanowires was observed over nanoparticles exhibiting specific discharge capacity of ~ 200 mAhg$^{-1}$ doubled as of $TiO_2$ (B) nanoparticulate layers.[17, 51] $MnO_2$ with different crystalline phases in 1D nanostructure as well as dendrite-like hierarchical forms were synthesized by hydrothermal method and found to be potential candidate as electrode in LIB.[52, 53] When $\alpha$- and $\gamma$-$MnO_2$ nanowire or nanorods exhibited good electroactivity to lithium ions delivering capacities more than 200 mAhg$^{-1}$, $\beta$-$MnO_2$ nanostructures showed low capacity and poor cyclic stability.[12, 52] Mn-oxide nanorods were also combined with graphene sheets showing four times higher capacitance for the nanocomposites compared to free $Mn_3O_4$ with 100% capacitance retention.[54] Xiao et al.[55] synthesized single crystalline iron oxide nanorods by simple calcination of $\alpha$-FeOOH precursor and observed very high reversible capacity of ~ 850 mAhg$^{-1}$ with more than 90% capacitance retention up to 50 cycles. Nanotubular structure exhibits even better lithium storage capacity with great reversibility due to thin tube wall, providing high Li$^+$ ion access area and inner hollow space, facilitating strain accommodation during charge/discharge process. Polycrystalline $\alpha$-$Fe_2O_3$ nanotubes (dia: 50–200 nm, shell thickness: 10–20 nm) were successfully synthesized by template-engaged precipitation of $Fe(OH)_x$ and followed by thermal annealing in air.[56] Such nanostructure when used as anode material in LIB exhibited considerably high capacities of

over 1000 mAhg$^{-1}$ with superior capacity retention at 0.5 C, almost doubled in compared to $Fe_2O_3$ nanoparticles. Several reports are available comparing the bulk vs. 0D vs. 1D nanostructures based on vanadium pentoxide ($V_2O_5$).[57-62] However, due to higher working potential value it is mostly used as efficient cathode electrode in LIB.

**Core-shell Nanostructures**. The fabrication of hollow sphere and core-shell nanostructures of same or different materials provided another good alternative as stable nanostructured anodes. In case of hollow spheres, inner void provide the necessary space for volume expansion during charging-discharging process. In contrary, the outer sphere in core-shell nanostructure deliver extra mechanical stability against the expansion-contraction of inner core material allowing surface permeability.[63-66] Mostly, template-assisted approaches are found to be useful for the fabrication of hollow as well as core-shell nanostructures with great control over their size and shape.[66, 67] Lou and his co-workers fabricated $SnO_2$ hollow nanosphere using mesoporous silica as nanoreactor.[68, 69] Mesoporous silica was used here as template and Sn-precursor was introduced through the hollow cavity of silica followed by thermal annealing to prepare $SnO_2$ inside the silica nanoreactor and finally etching out of silica outer sphere using HF solution.
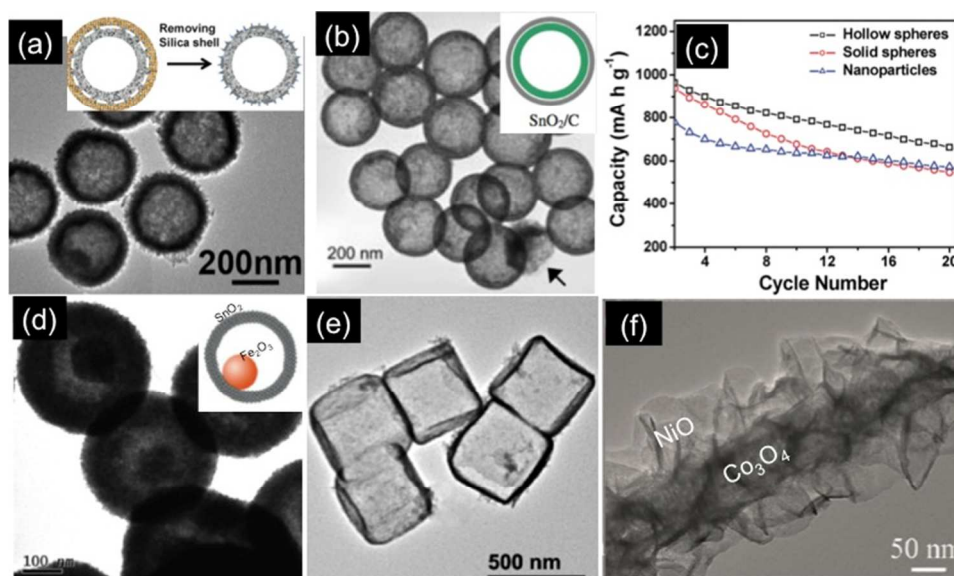


**Fig. 7**: (a-b, c-f) TEM images of (a) $SnO_2$ hollow sphere. Reprinted with permission from ref 68. Copyright 2011 American Chemical Society. (b) SnO2/C hollow spheres. Reprinted with permission from ref 43. Copyright 2009 John Wiley and Sons. (d) $\alpha$-$Fe_2O_3$@$SnO_2$ nano-rattles (Ref 71). (e) TEM image of as-prepared $SnO_2$ nanoboxes. Reprinted with permission from ref 66. Copyright 2011 American Chemical Society. (f) $Co_3O_4$/NiO core/shell nanowire. Reprinted with permission from ref 72. Copyright 2011 American Chemical Society. (c) comparison of cycling performances of $SnO_2$ hollow spheres, solid spheres and nanoparticles at a current rate of 160 mAg$^{-1}$ with a voltage window of 0.01-2.0 V Reprinted with permission from ref 68. Copyright 2011 American Chemical Society.

A comparative study showed that hollow spheres exhibit good capacitance stability as expected of ~ 750 mAhg$^{-1}$ at a current rate of 160 mAg$^{-1}$ up to 20 cycles in compared to solid spheres or nanoparticles. The work was further extended designing $SnO_2$@carbon coaxial hollow spheres by template-assisted method followed by hydrothermal method for making carbon outer sphere. Such nanoportal showed enhanced Li-ion diffusion, enhancing the charge rate capabilities with stable capacity ~ 500 mAhg$^{-1}$ at current rate of 625 mAg$^{-1}$ for at least 200 cycles. Another remarkable work was reported on fabrication of $SnO_2$ hollow nanobox by template-engaged coordinating etching of pregrown $Cu_2O$ nanocubes.[66] The

controlled hydrolysis of Sn$^{4+}$ in an optimum ethanol:$H_2O$ ratio decides the volume of nanoboxes. The structure found to be suitable to use as anode electrode in LIB. While the thin wall allows easy Li-ion diffusion, the inner hollow space able to accommodate volume variations during Li-ion insertion/extraction process. Though the initial discharge and charge capacities were very high (2242 and 1041 mAhg$^{-1}$), it decreased to 570 mAhg$^{-1}$ and remained stable up to 40 cycles. Moreover, template-free approach were reported by the same research group for the fabrication of $SnO_2$ hollow spheres by hydrothermal method and almost 75% greater charge capacity of 1140 mAhg$^{-1}$ were observed in comparison to

This journal is © The Royal Society of Chemistry 2014

*J. Mater. Chem.* A, 2014, **00**, 1-3 | 6

nanoparticles.[43] Lou et al.[70] synthesized $\alpha$-Fe$_2$O$_3$ hollow sphere by hydrothermal method via glycerol/water quasiemulsion-templating mechanism and manifested greatly enhanced Li storage property with very high reversible capacity of 710 mAhg$^{-1}$, even after 100 cycles. $\alpha$-Fe$_2$O$_3$@SnO$_2$ rattle-type hollow structures were also fabricated by the same research group by hydrothermal method via inside-out Ostwald ripening mechanism.[71] With the progress of reaction small crystallites in the interior dissolved out and re-deposited on the outer shell leading to an enlarged hollow interior space accompanied by construction of a compact shell. Such nanostructure leads to much lower initial irreversible loss and higher reversible capacity compared to SnO$_2$ hollow spheres. Co$_3$O$_4$/NiO core/Shell nanowire arrays on conductive substrates were fabricated by hydrothermal method followed by chemical bath deposition technique for NiO coating as reported by Xia et al.[72] Both the structural feature as well as the combination of materials results a high specific capacitance of 853 Fg$^{-1}$ at 2 Ag$^{-1}$ after 6000 cycles and an excellent cycling stability. Self-assembled porous NiO-coated ZnO nanorod electrodes were prepared on stainless steel substrate by hydrolysis of aqueous nickel chloride in the presence of hexagonal ZnO nanorod template followed by heat treatment to convert Ni(OH)$_2$ to NiO.[73] The thin porous NiO shell acts as a buffer layer, which primarily react with lithium ion and allows the ions to reach ZnO core. Such coating also helps to provide the structural integrity as well as enhance the electron conductivity of the electrode. The effects were clearly observed by significant improvement of reversible capacity value ~ 1100 mAhg$^{-1}$ for NiO-coated ZnO nanorod arrays in compared to ZnO nanorod arrays with ~ 700 mAhg$^{-1}$ and 1C current rate up to 15 cycles. Very recently, high-performance 3D electrodes for LIB consist of TiO$_2$–C/MnO$_2$ core–double-shell nanowire arrays were reported by Liao et al.[74] The complex structure was fabricated on flexible Ti-foil by layer-by-layer deposition with soaking process followed by glucose-assisted hydrothermal method and calcination for carbon coating and finally via redox reaction with KMnO$_4$ solution to deposit MnO$_2$ nanoparticles on the surface. The 3D electrode exhibit enhanced electrochemical performance with a higher discharge/charge capacity, superior rate capability, and longer cycling lifetime. Figure 7 represents various examples of hollow spheres and core-shell nanostructures as anode electrode in LIB.

**Heterogeneous Nanostructures.** An extension of core-shell nanostructure to hybrid branched nanostructures is of great interest. Such special structural features with tunable 3D morphology, homo or heterogeneous junction, provide structural integrity, high surface areas and direct electron transport pathways and thereby represent a unique system for applications in energy storage devices.[75, 76] Usually, the branched hybrid nanostructures are fabricated with the help of vapour phase, solution phase or by the combination of both methods. Interconnected porous MnO nanoflakes were grown on nickel foam by a reduction of hydrothermal synthesized MnO$_2$ precursor in hydrogen and the architecture proved to be potential candidate for lithium ion batteries showing very high specific capacity value of 700 mAh/g at the current density of 246 mA/g.[77] Fan and his co-workers[75, 78] fabricated $\alpha$-Fe$_2$O$_3$ nanorod branches grown epitaxially on SnO$_2$ nanowire stems by the combination of chemical vapour deposition (for the SnO$_2$ stem) and a hydrothermal route (for the FeOOH branches) followed by annealing to convert FeOOH to $\alpha$-Fe$_2$O$_3$. $\alpha$-Fe$_2$O$_3$/SnO$_2$ hybrid structure showed enhanced performance as anode in LIB with low initial irreversible loss and high

reversible capacity in comparison to both single components due to the synergetic effect exerted by SnO$_2$ and $\alpha$-Fe$_2$O$_3$. Another very promising hetero-nanostructure was reported by Wang et al.[79] composed of Si coated TiSi$_2$ nanonets, where Si acts as an active component to store and release Li$^+$ ion and TiSi$_2$ serves as the inactive component to support Si and to facilitate charge transport. The TiSi$_2$ nanonets were first grown on Ti-foil by chemical vapour deposition method using TiCl$_4$ and SiH$_4$ as the precursors[80, 81] followed by the flow of SiH$_4$ precursor for Si deposition on the TiSi$_2$ nanonets in the same method. The heteronanostructure showed remarkable performance with specific capacities >1000 mAh/g at a charge/discharge rate of 8400 mA/g along with long capacity life up to 100 cycles.
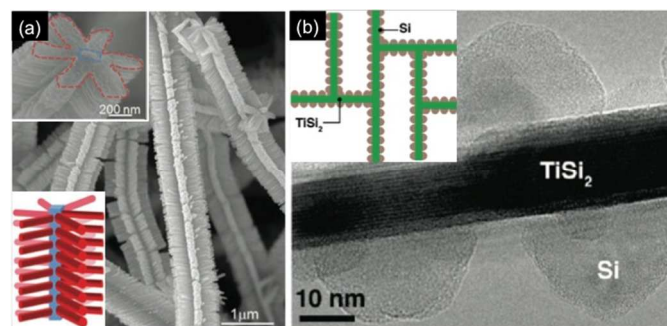


**Fig. 8**: (a) SEM image of $\alpha$-Fe$_2$O$_3$/SnO$_2$ branched nanostructures (*inset*: TEM image (top), schematic (below) of branched structure). Reprinted with permission from ref 77. Copyright 2011 John Wiley and Sons. (b) TEM image of Si nanoparticles deposited on TiSi$_2$ core (inset: schematic of heterostructure). Reprinted with permission from ref 78. Copyright 2010 American Chemical Society.

## 4. Types of Anode Materials

### 4.1 Carbonaceous Material

Carbonaceous material were the primary choice and known to be commercially most successful anode material in LIB having higher specific charges and more negative redox potentials than metal oxides, chalcogenides, and polymers.[82] They could be categorized in different forms: graphite/graphitized material, Non-graphitized soft carbon and hard carbon, each having different structures as well as electrochemical properties.

Graphite is considered to be layered structure containing carbon hexagon network in an orderly arrangement and sometime containing defects. The stacks are oriented in a specific A-B-A orientation, which on lithium intercalation changed to A-A-A orientation.[10] A defect-free ideal graphitic structure is very rare and thereby artificially manufactured, close to the graphite structure, polycrystalline carbon material, called as highly ordered pyrolytic graphite (HOPG) are commonly used. HOPG is synthesized by vapor transport method, a slow and expensive process.[83] Lithiunm intercalation entirely depends on the crystallinity, microstructure and morphology of the materials and thereby determines the lithiation-delithiation potential. The intercalation process occurs with the formation of Li-carbon alloys, Li$_x$C$_n$ in a reversible reaction:

$$Li_xC_n \underset{discharge}{\overset{charge}{\rightleftharpoons}} xLi^+ + xe^- + C_n\,(n = 6) \qquad (3)$$

This journal is © The Royal Society of Chemistry 2014

*J. Mater. Chem.* A, 2014, **00**, 1-3 | **7**
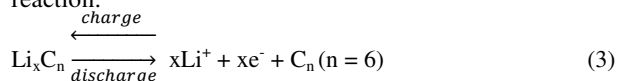
Highly crystalline graphitic carbon materials can intake one Li atom per six C-atoms in a completely reversible process with the theoretical capacity value 372 mAg/h. Lithium insertion and distribution into the layers of graphite occurs in several stages. At stage 1 lithium is distributed between all of the graphene layers; at stage 2, structure has an empty gallery between each occupied gallery, and a stage 4 structure has four graphene layers between each gallery containing lithium.[10, 82] However, several factors, like, SEI formation and the solvated lithium insertion in the graphene layers affects the reversibility of the intercalation reaction, increase cell resistance and thereby decrease the power density with number of cycles.[82]

Soft carbon is amorphous in nature and can be prepared by pyrolysis of organic polymers or petroleum pitch at ~ 1500 °C and available in the form of coke or carbon black. Such carbon materials are also known as 'low specific charge non-graphitic carbon' having x ~ 0.5 – 0.8 in $Li_xC_6$ where as x = 1 for graphite. On heating at high temperature, graphitizing carbons developed with weak crosslinking between layers. At 2500-3000 °C, enough crosslinking in between layers develops and thereby the material becomes mechanically harder than normal graphite, known as hard carbon. Such materials are also known as 'high specific charge carbonaceous material' having x ~ 1.2 – 5 in $Li_xC_6$ with high Li-storage capacity value of 200–600 mAhg[-1] and good power capability.[82] However, poor electrical conductivity and large irreversible capacity limits their extensive use as anode material in LIB.[64] Moreover, lithium diffusion entirely depends upon the crystal structure of carbonaceous material and it is believed that the process is facilitated by the presence of defects.[84]

The fact drives the use of bulk carbonaceous material to nano-carbon materials in different dimensions, say carbon nanotubes (CNT), carbon nanofibers (CNF) as 1D; graphene nanosheets as 2D; and porous carbon with pore size in nanometer range.

**1D carbon nanostructure**. CNTs are considered to be potential material having its characteristic $sp^2$ hybridization, high surface area, conductivity and fast 1D ion transportation. CNTs are prepared by rolling up the graphene layers by various methods - acid oxidation,[85, 86] ball milling,[87, 88] chemical vapour deposition[89-91] etc. in the form of single-walled CNT (SWCNT) or multiple-walled CNT (MWCNT) based on the morphological requirement. On decreasing the diameter of CNT, strain is generated, which causes the delocalization of electron making more electronegative than the bulk graphite.[92] As a consequence, the degree of lithium intercalation is increased, which is also reflected by high reversible capacity value up to 1116 mAg/h. Though in case of MWCNT the inter-wall distance can accommodate lithium ions during intercalation process, an increase of irreversible capacities and decrease in coulombic efficiency are observed due to the barrier for the extraction of lithium ions during discharging process.[91, 93] In order to overcome such difficulties, several reports are available on making hybrid materials with other metal oxides,[94, 95] chalcogenides[96, 97] or other form of carbonaceous materials.[98] Carbon nanofibres (CNF) are also used in place of CNTs as anode material in LIB, which can be synthesized by cost-effective and simple techniques, like, vapour deposition, arc discharge, laser ablation or electrospinning technique.[99-102] Though the irreversible capacity loss cannot be avoided for CNFs, the high rate capability can be achieved due to the greater reduction of lithium diffusion length in presence of surface as well as lattice defects in CNF.[102] However, an improvement of cyclability of reversible capacity of CNFs were

attained by Deng et al.[103] synthesizing carbon nanofibers with dome-shaped interiors by the noncatalytic thermal decomposition of acetylene under optimum condition. Other than morphological modification, making of nanocomposite materials are also well known approach to enhance the electrochemical properties with high reversible capacity and adequate stability.[104-108]

**2D carbon nanostructure**. A considerable amount of research work was also carried out using graphene nanosheets as 2D carbonaceous anode material in LIB, solely or in hybrid form. The fact of being one of the most useful anode materials is mainly due to the one atomic layer thick aromatic carbon network with high conductivity, great chemical, physical, mechanical properties and very high lithium storage ability having high surface area as it can accommodate lithium ions in both side of the sheet as well as at the edges, disorder defect sites.[92] Though, graphene nanosheet structure, unlike CNTs and CNFs, is no way associated with any lithium ion extraction barrier due to its structural design, it exhibits an unavoidable irreversible capacity and low Coulombic efficiency. It is noted that the charge capacity value in first cycle corresponds to 1233 mAhg[-1]. However, the discharge capacity decreased to 672 mAhg[-1] with Coulombic efficiency loss of 55%, while maintaining a reversible capacity value in the range of 500 mAg/h up to 30 cycles.[92] Such electrochemical properties can be explained by the undesirable chemical reactions of lithium ions with oxygen containing functional groups and formation of SEI on the defect sites. Moreover, insertion of electrolytes along with the lithium ions in between the layers is also responsible for such electrochemical behavior.[82, 92, 109] Moreover, the storage capacity alters with the interlayer spacing of graphene layers as well as functional groups present on the surface of the nanosheets, depending on the synthetic procedures.[110] Generally, graphene nanosheets are prepared by mechanical exfoliation to obtain nearly perfect graphitic nanostructure to be used in different electronic devices.[111, 112] In a solution method, chemical oxidation of natural graphite to graphene oxide (GO) followed by its reduction remains one of the most commonly used method to synthesize graphene nanosheets. The insertion of oxygen containing functional group during the process found to have a detrimental effect on lithium ion storage capacity decreasing the reversible capacity value sometimes even less than that of natural graphite.[110, 113] This can be confirmed from GO nanosheets with low reversible capacity value of 335 mAhg[-1], which under reduction process shows a significant improvement up to ~ 1000 mAhg[-1] with good capacity retention as shown in Fig. 9(e). A high reversible capacity value was achieved for graphene nanosheet with a large interlayer distance of ~ 4 Å due to increase of available sites for lithium ion accommodation as reported by Yoo et al.[114] In another report, improvement of reversible capacity up to 780 mAhg[-1] by combining CNTs and $C_{60}$ has been noted. Recently, high and stable reversible capacity has been achieved by fabricating nanocomposites of graphene with metals and metal oxides. Accordingly, active metals, like, Si[115], Sn[116]-based graphene nanocomposites are found to be promising material. In addition, metal oxides, e.g., $Co_3O_4$,[117-119] $TiO_2$,[37, 120, 121] $Fe_3O_4$,[122-128] $Mn_3O_4$,[129, 130] CuO,[131] NiO[132] and $SnO_2$[133] nanoparticles, anchored on the surface of graphene nanosheets, also successfully diminish the irreversible capacity loss during charging-discharging process. Such improvement in the electrochemical properties of materials is attributed to the synergistic effect of graphene and metal or metal oxide nanoparticles. When graphene nanosheets provide high surface

area as well as high conductivity, anchoring of electroactive metal or metal oxide nanoparticles on the nanosheet surface prevents the coagulation of stacks facilitating the lithium storage in a greater extend.

**3D porous carbon nanostructure.** Porous carbon nanostructures with different range of pore sizes are known to be another alternative anode material for LIB. Generally, depending upon the pore size they can be categorized as microporous (< 2 nm), mesoporous (2-50 nm) and macroporous (> 50 nm) carbonaceous material. They show excellent electrochemical properties due to very high surface areas and interconnected carbon network allowing super conductivity as well as accommodating strain generated during charging-discharging process.[92] Usually the template-assisted synthetic methods or chemical treatment followed by pyrolysis of bulk materials are used to fabricate porous carbon nanostructure with different pore sizes.[134-137] Unlike 1D or 2D carbon nanostructures, the difficulty of irreversible capacity loss can be avoided significantly by utilizing porous carbon nanostructure. Zhou et al.[135] synthesized mesoporous carbon with uniform pore size of 3.9 nm by utilizing ordered silica SBA-15 as a template followed by carbonization of sucrose inside the pores. The material showed an excellent specific reversible capacity of ~ 1000 mAg/h at current rate of 100 mAg$^{-1}$ with good retention up to 20 cycles. However, in some cases very high surface area of material results considerable irreversible capacity loss as reported by Takeuchi et al.[137] They used zeolite and clay as templates to prepare the carbonaceous materials with very high surface area, which causes electrolyte decomposition and SEI formation on the carbon surface resulting an irreversible capacity loss from ~ 3500 mAhg$^{-1}$ to ~ 500 mAhg$^{-1}$ in the first cycle. However, after 1$^{st}$ cycle, the materials show stable reversible capacity with > 80% capacity retention values making them promising for anode material in LIB.

Very recently, Pint and his co-workers reported very high reversible capacities of 2640 mAhg$^{-1}$ at a current rate 0.186 Ag$^{-1}$ by designing anode material with freestanding, flexible graphene and carbon nanotube hybrid foams.[138] Such hybrid material showed high performance due to the decoupling of lithium storage reaction energetics dictated by the SWNTs from the total storage capacity of the hybrid material as well as developing mechanically robust carbon electrodes.
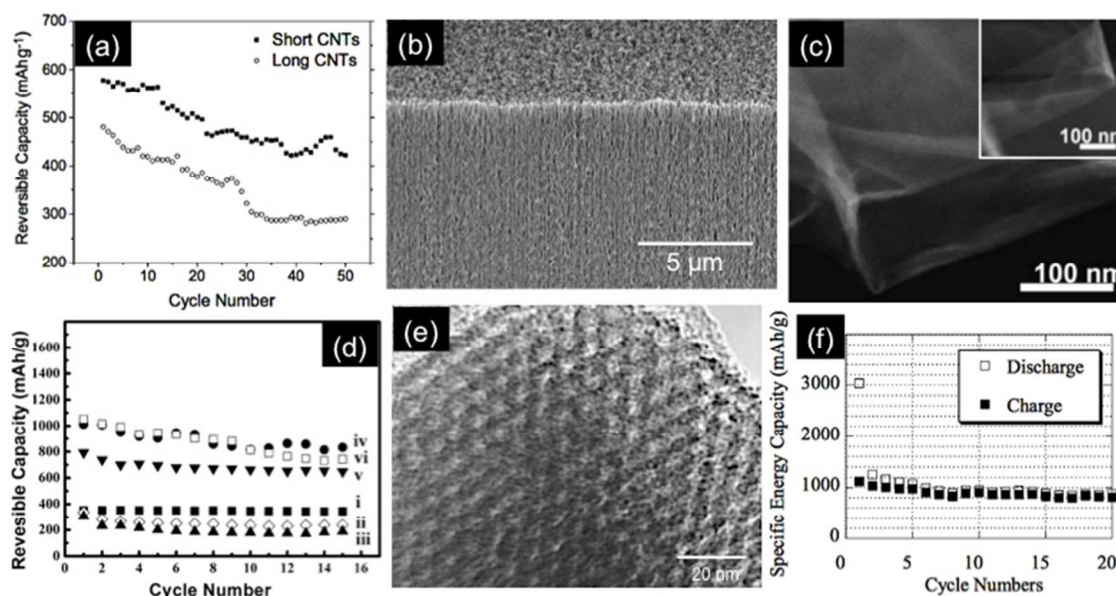


**Figure 9**: (a) Variation of C$_{rev}$ for short and long CNT with number of cycles at a current density of 25 mAg$^{-1}$. Reprinted with permission from ref 90. Copyright 2007 John Wiley and Sons. (b) SEM image of SWNT-forest. Reprinted with permission from ref 89. Copyright 2006 Nature Publishing Group. (c) TEM images of graphene nanosheets (*inset*: oxidized graphene). Reprinted with permission from ref 113. Copyright 2008 American Chemical Society. (d) Cyclic performance of natural graphite (i), pristine GO (ii), hydrazine-reduced GO (iii), 300ºC pyrolytic GO (iv), 600ºC pyrolytic GO (v), and electron-beam-reduced GO (vi) at a current density of 0.05 Ag$^{-1}$. Reprinted with permission from ref 109. Copyright 2009 American Chemical Society. (e) TEM image of ordered mesoporous carbon and (f) its discharge and charge cycle performance at a constant current of 100 mAg$^{-1}$. Reprinted with permission from ref 134. Copyright 2003 John Wiley and Sons.

## 4.2 Spinel Structured Li$_4$Ti$_5$O$_{12}$

Graphite, being a primary choice as anode electrode in LIB, shows the lithiation potential ~ 0.2 V vs. Li/Li$^+$, close to the lithium stripping voltage and especially at high rate, it may cause a safety issue.[10] Moreover, such a low lithiation potential range leads to the formation of electronically insulating solid-electrolyte interphase (SEI) on the surface of graphite, which likely to occur below 1.0 V versus Li/Li$^+$. The disadvantages of using graphite can be avoided by using spinel structured Li$_4$Ti$_5$O$_{12}$ as reported by Thackeray's group in 1994.[139] Unlike graphite, Li$_4$Ti$_5$O$_{12}$ works at a potential 1.5 V vs. Li/Li$^+$ and

thereby the SEI layer formation can be avoided. Moreover, it shows high specific capacity (~170 mAhg$^{-1}$), good cyclic stability due to zero strain or volume change during charging and discharging process.[12, 140] However, poor electronic conductivity (10$^{-13}$ S cm$^{-1}$) of Li$_4$Ti$_5$O$_{12}$ and moderate Li$^+$ diffusion coefficient (10$^{-9}$–10$^{-13}$ cm$^2$ s$^{-1}$) limits the performance, which up to a certain extend can be overcome by reducing size and conductive coating.[9, 141-144] Several reports are available on the size dependence performance of Li$_4$Ti$_5$O$_{12}$.[144-146] Jaiswal et al.[146] fabricated Li$_4$Ti$_5$O$_{12}$ with two different size distributions of 50 nm and 200 nm by pyrolysis method and exhibited charge capability values of 148 and 138

This journal is © The Royal Society of Chemistry 2014

*J. Mater. Chem.* A, 2014, **00**, 1-3 | 9

mAhg$^{-1}$ at C/25 and 5C, respectively. Other than nanoparticles, $Li_4Ti_5O_{12}$ in the form of hollow microspheres[147] and nanowire[148] structures also showed high performance gaining structural stability with more than 90% capacity retention.[12] Besides fabrication of nanostructured $Li_4Ti_5O_{12}$, conductive coating with carbon or surface nitridation approach also found to be fruitful for further improvement in their performances.[39, 40, 149] Ionic liquids, containing C, H and N elements, are commonly used precursor for N-doped carbon coating on to the surface of $Li_4Ti_5O_{12}$ as they can penetrate porous material easily due to their fluidic property.[39, 150] Such coated porous $Li_4Ti_5O_{12}$ materials show initial capacity of 150 mAhg$^{-1}$ at 2C, decreased to 124 mAhg$^{-1}$ after 2200 cycles at 2C, with very good capacity retention of 83%. Figure 10 shows an example of C-coated $Li_4Ti_5O_{12}$ and comparison of cycling performance of coated and uncoated $Li_4Ti_5O_{12}$ sample.
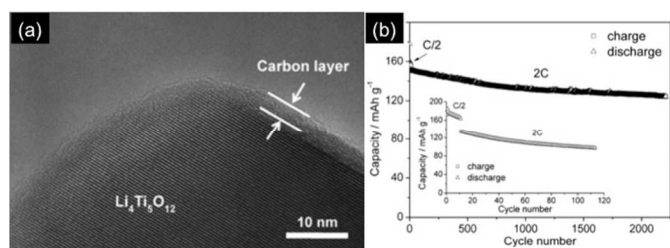


**Fig. 10**: (a) TEM image of 5 wt % pitch-coated $Li_4Ti_5O_{12}$. Reprinted with permission from ref 40. Copyright 2011 Elsevier. (b) Comparison of cycling performance of N-doped carbon coated and pristine (inset) $Li_4Ti_5O_{12}$. Reprinted with permission from ref 39. Copyright 2011 John Wiley and Sons.

### 4.3 Metal Alloys

The concept of binary metal alloys as effective electrode material for energy storage devices was first proposed by Huggin and Besenhard.[151, 152] Later on, extensive investigations were carried out in designing different metal as well as metal oxide alloys and evaluated their performances in LIB. The preliminary choice of metal alloys were Li-based alloys, $Li_xM$, where M used to be secondary metal electrochemically active or inactive.[153] The role of M was to provide the matrix of the alloy electrode to support the strain generated during lithium intercalation-deintercalation process as well as to improve the electrical conductivity.[154] However, disadvantages, like, decrease in reversible capacity value due to incorporation of electrochemically inactive material in alloys and volume expansion during charging-discharging process resulting cracks on the surface of alloys are noticed. In order to avoid such problems and to improve reversible capacity values with good cyclability, use of electrochemically active-active binary metal alloys in the nanodimensional structure have drawn much attention. In this context, electroactive metals, such as, Si,[155-158] Sn,[159, 160] Al,[161-163] Ga,[164] Ge,[165, 166] Pb,[167] Sb[168, 169] are extensively studied as matrix metals with the reversible formation of Li-M different phases including phase transitions in several steps during lithiation-delithiation process.[10, 82] The choice of metal matrices are based on their individual reversible capacity values as well as the phase diagrams and equilibrium thermodynamic properties.[10] Among these electroactive metals, Si is the most studied material as anode involving the alloy formation with lithium as $Li_{12}Si_7$, $Li_7Si_3$, $Li_{13}Si_4$, and $Li_{22}Si_5$ in several steps.[170] The formation of alloys with different phases is also accompanied by the crystalline-to-amorphous mechanism in a two step process during charging-discharging process as follows:[171, 172]

*During discharge:*

$$Si \text{ (crystalline)} + xLi^+ + xe^- \rightarrow Li_xSi \text{ (amorphous)} + (3.75-x)Li^+ + (3.75-x)e^- \quad (4)$$

$$\rightarrow Li_{15}Si_4 \text{ (crystalline)} \quad (5)$$

*During charge:*

$$Li_{15}Si_4 \text{ (crystalline)} \rightarrow Si \text{ (amorphous)} + yLi^+ + ye^- + Li_{15}Si_4 \text{ (residual)} \quad (6)$$
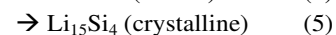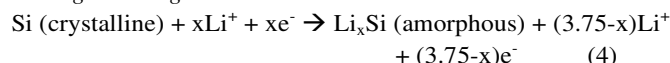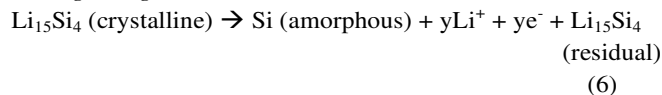
Though Si-based electrodes shows extremely high reversible capacity value, the unavoidable volume expansion of almost 400% due to lithiation remains one of major challenge. Several reports are available on this issue showing the morphological changes occur during lithiation-delithiation process.[156, 173] The use of different nanosized Si and its lithiation process is discussed in detail in the next section. Like Si, Sn metal undergoes reaction with Li and results formation of different Li-Sn phases as $Li_2Sn_5$, $LiSn$, $Li_7Sn_3$, $Li_5Sn_2$, $Li_{13}Sn_5$, $Li_7Sn_2$, and $Li_{22}Sn_5$. The most lithium rich Sn-Li alloy, $Li_{22}Sn_5$, can accommodate 4.5 atoms of Li per each Sn atom delivering the capacity value of 959.5 mAhg$^{-1}$ at working potential of 0.5 V vs. Li/Li$^+$.[153] Though reversible capacity value of Sn-Li alloy based anode is low in compared to Si-Li alloy system, the low melting point of Sn facilitates the alloy formation with Li as well as easy crystallization and also the mobility of Sn in alloy becomes easier than the other metals.[174] However, poor capacity retention due to inhomogeneous volume change with the formation of different intermetallic Li-Sn phases is observed during charging-discharging process.[153, 175] The capacity retention of Sn-based anode can be improved to a large extent by using the oxide form of Sn. Sn-oxides undergo reaction with Li forming $Li_2O$ and itself reduced into Sn according to the electrochemical reaction shown in reactions (14), (15). Though in the first cycle an irreversible capacity loss is observed due to the formation of electrochemically inactive $Li_2O$, afterwards good stability during several cycles are noticed. Such stability could be attributed due to the reversible Li-Sn alloy formation reaction with metallic Sn and Li$^+$ ion as well as due to the role of $Li_2O$ as a matrix preventing the aggregation of formed Sn nanoparticles. Lithium alloy formation is also well known for Al metal forming different phases of $Li_xAl$ alloys (0.1 < x < 1). Up to 50 at% of lithium content is reported in the Li-rich alloy accompanied by large extent of volume expansion.[161] Moreover, high ionic character of $Li_xAl$ alloys leads to the brittle nature of the material reducing mechanical stability.[82] A very good piece of work was reported by Huang and his group showing an *in situ* transmission electron microscopy observation of pulverization of aluminum nanowires during lithiation-delithiation cycles.[162] According to this, lithiation process started through the $Al_2O_3$ coating, forming a stable Li-Al-O glass tube, towards the Al nanowire core converting single crystal Al into polycrystalline LiAl alloy. Such alloy formation resulted 100% volume expansion accompanied by appearance of voids causing irreversible capacity loss from 800 to less than 200 mAhg$^{-1}$. Li-Ge alloy system has also found to be an interesting anode material showing the theoretical capacity of 1568 mAhg$^{-1}$ ($Li_{17}Ge_4$). Though the theoretical capacity value is much less in compared to Li-Si system, Ge is favoured due to very faster lithium diffusivity than Si.[176] Other group V elements, are also known to be promising material forming Li-rich alloy system, such as, $Li_3P$, $Li_3As$, $Li_3Sb$, and $Li_3Bi$ with high capacity values due to their low atomic packing factor in their crystal structure leading to large accommodation of Li-ions in the voids.[153]

This journal is © The Royal Society of Chemistry 2014

*J. Mater. Chem*. A, 2014, **00**, 1-3 | **10**

However, undesirable factors, like, large volume expansion, mechanical integration resulting significant irreversible capacity loss during lithiation-delithiation process cannot be avoided.

Another possible strategy for the alloy based anode material is the fabrication of intermetallic $M_1$-$M_2$ system, where $M_1$ and $M_2$ are either electrochemically active-active or active-inactive in nature.[153] It is believed that in case of electrochemically active-active intermetallic compound multiphases are generated during the lithiation process, in which two different phases mutually buffer each other preventing the volume expansion to some extent gaining the stability of the electrode. Moreover, the system involves the formation of a ternary alloy, Li-$M_1$-$M_2$ system during lithiation process with favourable voltage profile as well as reversible capacity values. For electrochemically active-inactive combination, the inactive metal acts as the metal matrix as in case of binary $Li_xM$ alloys. In both these categories, intermetallic compounds of Si and Sn with various metals are mostly studied. Mg or Ag-silicides are known Si-based intermetallic alloy compounds with Mg and Ag as electroactive elements. The complicated lithiation process involves the formation of both binary as well as ternary metal alloys Li-Si, Li-Mg and $Li_xMg_2Si$ respectively as follows proposed by Kim et al.:[177]

$$Mg_2Si + xLi^+ + xe^- \rightarrow Li_xMg_2Si \qquad (7)$$
$$Li_xMg_2Si + xLi^+ + xe^- \rightarrow Li_{critical}Mg_2Si \qquad (8)$$
$$\rightarrow Li_{saturated}Mg_2Si + Mg + Li–Si\ alloy \qquad (9)$$
$$Mg + xLi^+ + xe^- \rightarrow Li–Mg\ alloy \qquad (10)$$
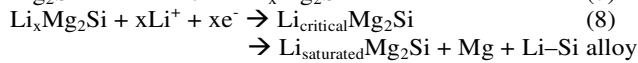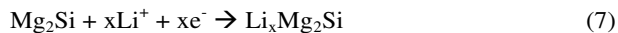
The insertion of $Li^+$ ion occurs in the octahedral sites of $Mg_2Si$ forming the ternary alloy compound $Li_xMg_2Si$, which can further accommodate $Li^+$ ion until it forms unstable $Li_{critical}Mg_2Si$ intermetallic alloy, which undergoes electrochemical reaction resulting $Li_{saturated}Mg_2Si$, Li–Si and Li-Mg alloys. The lithium insertion mechanism in SiAg alloy is also reported elsewhere showing a stable capacity of 280 mAhg$^{-1}$.[178] Mostly, such intermetallic alloy compounds are synthesized by mechanical ball milling process. Si–M (M = Ni, Fe, Co, Mn, Cr etc.) are the other examples of intermetallic alloys of Si, where the M is electrochemically inactive transition metals serving as a buffering matrix against the volume expansion during lithiation.[179-183] In such cases, the electrochemical reactions can be described as follows:

$$xLi^+ + xe^- + NiSi \rightarrow Li_xSi + Ni \leftrightarrow Ni + Si + xLi^+ + xe^- \qquad (11)$$
$$xLi^+ + xe^- + FeSi \rightarrow Li_xSi + Fe \leftrightarrow Fe + Si + xLi^+ + xe^- \qquad (12)$$
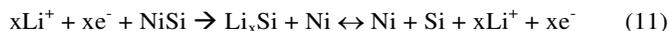
The capacity values (~60-1000 mAhg$^{-1}$) with good capacity retention depending upon the alloy compositions have been noted. Similar to Silicon (Si), intermetallic Sn-inactive M (M = Fe, Cu, Co, Cr, Mn, Ni etc.) alloys have also been applied in LIB.[184-191] Wang et al.[184] prepared $FeSn_2$, $Cu_6Sn_5$, $CoSn_3$, and $Ni_3Sn_4$ single-crystalline nanospheres of particle size ~ 40 nm by modified polyol process and their electrochemical properties were compared. The capacity values follow the order: $FeSn_2$ > $Cu_6Sn_5$ ≈ $CoSn_3$ > $Ni_3Sn_4$ with highest capacity for $FeSn_2$ (500 mAhg$^{-1}$). Such electrochemical behavior is attributed due to the structurally open channels in the $FeSn_2$ crystal lattice as well as SEI formation after the first cycle leading to superior cycling performance. Electrochemically active M-Sn intermetallic compounds, such as, SbSn,[192-194] $Ag_3Sn$,[195] and $Mg_2Sn$[196] are also reported, which involves ternary Li-Sn-M alloy formation

similar to Si-based intermetallic compounds. Very recently, Seo and Park fabricated nanostructured $SnSb/MO_x$(M = Al or Mg)/C hybrid material by mechanical milling technique via mechanochemical reduction of SnO and $Sb_2O_3$ with Al or Mg, respectively, in presence of carbon.[194] In this nanohybrid material, it is believed that SnSb acted as the active material, and $Al_2O_3$ or MgO as the inactive material with amorphous carbon as buffering matrix. The fact can be confirmed from their electrochemical analyses as SnSb particles showed very poor performance due to large volume change, which can be improved to a reversible capacity value ~ 500 mAhg$^{-1}$ with great stability up to 150 cycles for $SnSb/Al_2O_3$/C and SnSb/MgO/C nanocomposite electrodes.
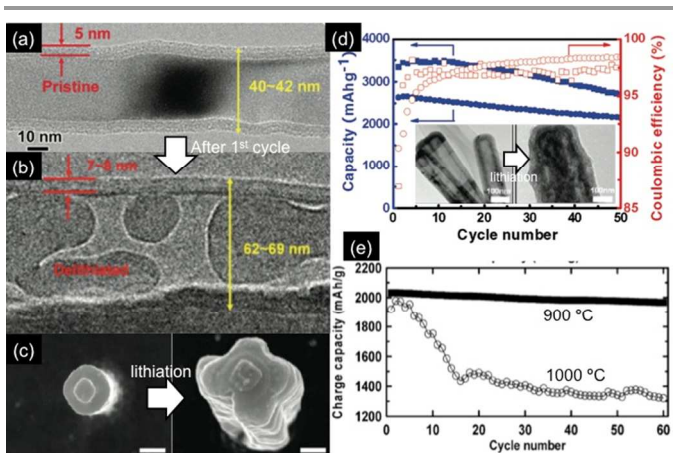


**Fig. 11**: (a-b) An in-situ TEM observation of pristine $Al_2O_3$ coated Al NW morphology before (a) and after (b) lithiation-delithiation showing the pulverization and volume expansion of the Al NW. Reprinted with permission from ref 161. Copyright 2011 American Chemical Society. (c) SEM top view of crystalline (100) Si nanopillars showing anisotropic lateral expansion after full lithiation. Reprinted with permission from ref 155. Copyright 2011 American Chemical Society. (d) Cycle performances of Si NT array electrode at a rate of 0.05 and 0.2 C (square symbol: 0.05 C, circle symbol: 0.2 C). Reprinted with permission from ref 172. Copyright 2011 American Chemical Society. (e) charge capacity vs. cycle number of $Si_{70}Sn_{30}$ nanoalloys annealed at 900 and 1000 ºC in coin-type half cells between 1.2 and 0 V at a rate of 0.2 C (= 1000 mAg$^{-1}$) (Ref 200).

Other than Si or Sn based intermetallic compounds, intermetallic alloys, like $Cu_2Sb$,[197] $CoSb_3$,[198] $ZnSb$[199] are also promising material for LIB application. Saadat and his group synthesized different ZnSb nanostructures in the form of nanoflakes, nanowires, or nanoparticles with tunable Zn:Sb molar ratios by electrochemical deposition techniques and compared their performance as anode electrode in LIB.[199] The study revealed that the ZnSb nanoflakes found to be superior to nanowire or nanoparticle structures of same compositions and phases with high Li-ion storage capacities of 500 mAhg$^{-1}$ and stable cyclabilities up to 70 cycles, with a Coulombic efficiency of 98%. Another approach involved the improvement in irreversible capacity loss of intermetallic alloys and cyclic stability with good capacity retention by the formation of composite of intermetallic nanoalloys with carbon.[200-203] Cho and his co-workers fabricated carbon-coated $Si_{70}Sn_{30}$ nanoalloys by vacuum annealing butyl-capped analogues at 900 ºC, and showed an outstanding high reversible capacity of 2032 mAhg$^{-1}$ with capacity retention of 97% after 60 cycles.[201]

### 4.4 Silicon based Materials

Silicon is another promising anode material with low discharge potential of ~ 370 mV vs. Li/Li$^+$.[204] It can accommodate 4.4 lithium atoms per single Si atom forming an alloy Li$_{4.4}$Si providing very high theoretical specific capacity value (4212 mAhg$^{-1}$), which is ten times higher to the conventional graphite and stable voltage during cycling.[47, 205] However, the use of silicon still remains challenging due to large volume expansion (> 400%) during lithiation-delithiation process and formation of SEI layer at low potential. It may be noted that the volume expansion of bare Si causes poor reversibility and rapidly declining capacity. It can be managed by alloying with other material to minimize the stress inside the material or by fabricating 1D nanostructure of Si to accommodate the strain generated during several cycles.[47, 206-208] Though, SEI layer formation provides mechanical stability against the electrode expansion, is responsible for irreversible capacity loss influencing the kinetics of lithium ion transfer between the electrolyte and the electrode. Si nanoparticles are mostly synthesized by ball milling, pyrolysis method or via template-assisted method.[209-211] Usually either Si/C composite materials

or carbon additive binders are mixed with Si nanostructures to improve electrical conductivity to the current collector.[207, 212, 213] Li et al.[209] synthesized Si nanoparticles (dia: 78 nm) and combined with carbon binders and showed a high reversible capacity of 1700 mAhg$^{-1}$ at a cycling voltage between 0.0–0.8 V. Mazouzi et al.[210] also observed reversible capacity of 960 mAhg$^{-1}$ with excellent stability over 700 cycles using Si particles and carboxymethyl cellulose binder composite material. Kim et al.[211] synthesized well-dispersed n-Si nanoparticles (size range: 5-20 nm) in presence of surfactant followed by carbon coating by flowing acetylene gas through the products at high temperature and studied their performance as anode in LIB. It was inferred that 10 nm sized nanoparticles showed significantly high charge capacity of ~ 3400 mAhg$^{-1}$ with capacity retention of 81%, which could be further improved to 96% after carbon coating up to 40 cycles (Fig.12a-b). Si nanowires/nanotubes grown on conductive substrate by vapour deposition method found to be very efficient for this purpose.[47, 214] They can accommodate large strain without pulverization, provide good electronic contact and conduction.
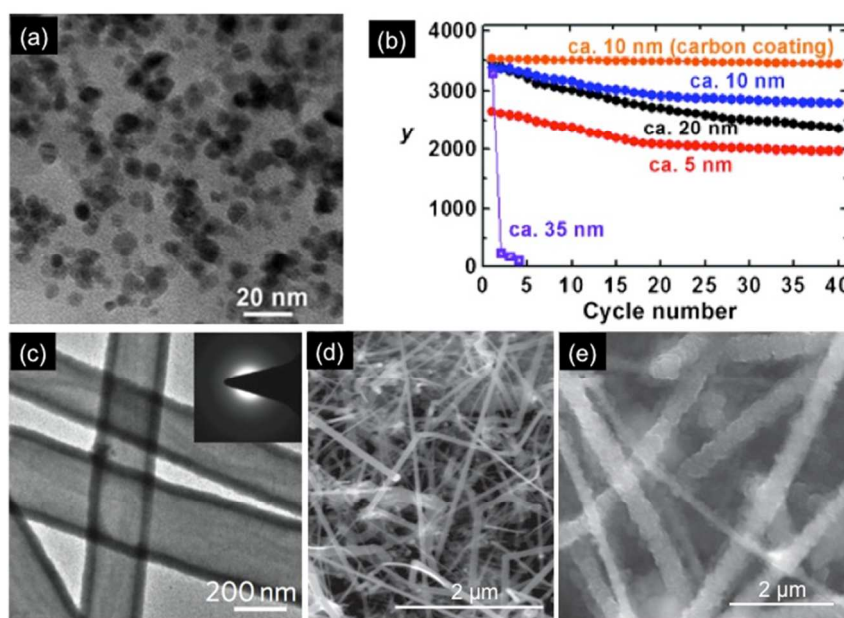


**Fig. 12**: (a) TEM image of 10 nm sized n-Si nanoparticles, (b) comparison of charge capacity of different sized n-Si nanoparticles. Reprinted with permission from ref 210. Copyright 2010 John Wiley and Sons. (c) TEM image of double walled Si nanotubes. Reprinted with permission from ref 215. Copyright 2012 Nature Publishing Group. (d-e) SEM images of pristine Si NWs before (d) and after (e) electrochemical cycling. Reprinted with permission from ref 47. Copyright 2012 Nature Publishing Group.

Cui and his group carried out extensive studies on 1D nanostructured Si and its composite materials with superior electrode design.[47, 215-217] The Si nanowires grown on stainless steal showed very high specific capacity of ~ 3500 mAhg$^{-1}$ with capacity retention of 75% where double walled Si nanotubes showed the specific capacity charge of ~1500 mAhg$^{-1}$ at rate of C/5 with an outstanding stability of 6000 cycles with cycled time of more than one year.[47, 216] Song et al.[173] fabricated sealed Si nanotube arrays that is capable of accommodating large volume changes associated with lithiation process. The geometry exhibited very high and stable charge capacity value of over 3000 mAhg$^{-1}$ at the current rate of 0.1 C. The surface structure becomes rough during electrochemical cycling (Fig. 12d-e) with increased electrical resistivity due to crystalline-to-

amorphous transition.[215] Therefore, desired electrical conductivity as well as the structural integrity could be maintained by applying hybrid nanostructure. Cao et al.[218] fabricated Cu-Si-Al$_2$O$_3$ nanocables directly grown on current collector. While the Cu core provides inner mechanical stability and maintains electrical conductivity, the outer sheath of Al$_2$O$_3$ provides a stable Si/electrolyte interface and triggers stable SEI formation. Such nanocables deliver a specific capacity of ~1560 mAhg$^{-1}$ under a current density of 1.4 Ag$^{-1}$ up to 100 cycles. Wang and his group synthesized a unique heteronanostructure consist of two-dimensional TiSi$_2$ nanonets as mechanical supporter and particulate Si coating as electroactive material.[79, 219] The heteronanostructures showed specific capacities >1000 mAhg$^{-1}$ at a charge/discharge rate of 8400 mAg$^{-1}$ with only an

This journal is © The Royal Society of Chemistry 2014

*J. Mater. Chem.* A, 2014, **00**, 1-3 | **12**

average of 0.1% capacity fade per cycle up to 100 cycles. Fan and his co-workers fabricated vertically ordered $Ni_3Si_2/Si$ nanorod arrays directly grown on current collector. In this geometry, Si acts as electroactive material and $Ni_3Si_2$ as inner mechanical supporter.[220] The structure showed high and steady discharge capacity of over 2184 mAhg$^{-1}$ up to 50 cycles. Synthesis of nanostructured layered silicon-germanium systems $(Si_{1-x}Ge_x)$ were also attempted by glancing angle deposition (GLAD) method.[221] The material offered very high reversible capacity of > 2000 mAhg$^{-1}$ at very high rate (20 C) as lithium ion battery anodes.

### 4.5 Transition Metal Oxides and their Composites

Transition metal oxides (TMO) are found to be potential substitutions of graphite as anode material in LIB due to very high specific capacity values of $3d$ metal oxides. In addition, the lithium ion reacts reversibly with metal oxides avoiding metal-lithium alloy formation as follows:[9, 222]

$$MO + xLi^+ + xe^- \leftrightarrow Li_2O + M \; (M = Fe, Co, Ni, Cu) \quad (13)$$

The forward reaction is thermodynamically favorable and involves multiple electron transfer per unit metal atom leading to high theoretical lithium storage capacity. However, the reaction in the backward direction, i.e., formation of $Li^+$ ion from $Li_2O$ is thermodynamically unfavorable process and is believed to be facilitated by metal nanoparticles (M) formed during reaction.[63] This indicates the reversibility of the reaction is well maintained in the nanoscale system. Other limitations, like, poor conductivity, low diffusion coefficient and formation of thick SEI layer could be overcome by attaining different combination of materials or by fabricating different hierarchical nanostructures.

Among different TMOs, tin oxide ($SnO_2$) was the preliminary choice of using as anode material due to its high theoretical capacity values of 790 mAhg$^{-1}$.[223, 224] The major drawback of using $SnO_2$ as anode material in LIB is the irreversible nature of the reaction with lithium ion leading to large capacity loss initially. However, metallic Sn formed in the next step undergo reversible alloy formation accommodating 4.4 Li atoms per single Sn atom, which is further affected by the large volume change during lithiation process.[63, 225, 226]

$$SnO_2 + 4Li^+ + 4e^- \rightarrow Sn + 2Li_2O \quad (14)$$
$$Sn + xLi^+ + xe^- \leftrightarrow 4Li_xSn \; (0 \leq x \leq 4.4) \quad (15)$$
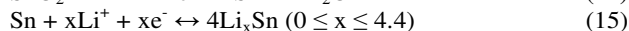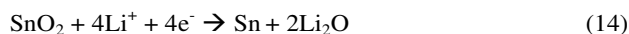
It is noteworthy that hollow spheres, core-shell or mesoporous structures of $SnO_2$ can accommodate the volume change,[43, 226] whereas $SnO_2$ in the form of nanowires, nanorod structures provide the mechanical support to sustain during several cycles of intercalation-deintercalation process.[48] Titirici et al.[226] employed hydrothermal carbonization process to synthesize mesoporous $SnO_2$ microspheres via nanoparticles assembly. It is noted that the porosity not only helps the faster lithium intercalation-deintercalation process, but also provide good network system making the surfaces available for electrolytes. The mesoporous structure showed the specific capacity of 370 mAhg$^{-1}$ at the current density 1 Ag$^{-1}$
. Lou and his group carried out an extensive study on fabricating different hollow $SnO_2$ nanostructures and investigated their lithium storage capacity in LIB.[43, 66-69, 71, 227] Hollow $SnO_2$ nanoboxes, prepared by template-engaged coordinating etching of pre-grown $Cu_2O$ nanocubes, found to be promising material.[66] They showed the capacity value of about 570 mAhg$^{-1}$ over 40 cycles at a current rate of 0.2C. In

order to attain high as well as stable capacity values, fabrication of 1D nanostructures grown directly onto the current collector were also attempted by Kim et al.[48] They synthesized 1 μm long $SnO_2$ nanowires with the diameter range of 40-50 nm by vapor–liquid–solid (VLS) mechanism. When it was directly used as anode material in LIB, > 700 mAh/h discharge capacity at a current density of 782 mAg$^{-1}$ stable up to 50 cycles was observed. On the contrary, $SnO_2$ nanopowders undergoes a steady deterioration of discharge capacity values with cycle numbers. Hybrid $SnO_2$ nanowires encapsulated by Sn nanoclusters have also been explored as an excellent anode electrode in LIB by Sunkara and his co-workers.[228] The electrode exhibited an exceptional capacity of > 800 mAhg$^{-1}$ over 100 cycles with a low capacity fading of less than 1% per cycle. However, post lithiation analyses after 100 cycles showed little morphological degradation of the hybrid nanowires. Liu et al.[229] synthesized $SnO_2$ nanorods of 60 nm in diameter and 670 nm in length directly grown on metal or metal alloy substrates via alkaline hydrothermal methods. Such array electrode showed specific capacity value of 580 mAhg$^{-1}$ after 100 cycles at 0.1C, with coulombic efficiency of nearly 100%.

Titanium dioxide ($TiO_2$) is another promising anode material in LIB due to its non-toxic, ecofriendly nature and abundant availability. Though $TiO_2$, due to its photocatalytic activity, are extensively used in numerous applications, e.g. dye-sensitized solar cell, water splitting, photocatalysis, gas sensing etc.[230-232] A considerable amount of work has also been done in LIB with the theoretical specific capacity value of 335 mAhg$^{-1}$. The lithium intercalation-deintercalation occurs in the interstitial positions of $TiO_2$ crystals with the lower cut off potential of 1.0 V vs. $Li^+/Li$ and can be presented as the following reversible reaction:

$$xLi^+ + TiO_2 + xe^- \leftrightarrow Li_xTiO_2 \; (0 \leq x \leq 1) \quad (16)$$
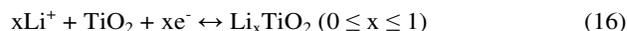
A phase transition from tetragonal to orthorhombic $TiO_2$ is observed due to lithium intercalation. $TiO_2$ exists different polymorphs, such as, anatase, rutile, brookite, $TiO_2$ B (bronze), $TiO_2$ H (Hollandite) etc. and the electrochemical activity depends upon the their intrinsic properties based on their crystal structures. Among different polymorphs, anatase $TiO_2$ is known to be most electro active material.[63, 233] In all cases the $Li^+$ ion diffusion is highly anisotropic and occurs along $c$-axis. Though the mechanism leads fast $Li^+$ ion diffusion in anatase $TiO_2$, but in rutile the diffusion is inhibited due to its crystal orientation.[9] The performance of rutile $TiO_2$ can be improved by preparing nanosized rutile $TiO_2$ showing specific capacity of 132 mAhg$^{-1}$ at 1C with good retention as reported by Hu et al.[19] Moreover, anatase $TiO_2$ with higher percentages of (001) exposed facets is more reactive than (101) facets and undergoes fast reversible lithium intercalation-deintercalation reaction.[234-236] However, poor electrical conductivity limits extensive use of pristine $TiO_2$ in LIB. The conductivity can be improved by N-doping of $TiO_2$.[237] The 1D mesoporous $TiO_2N_x$ exhibited specific capacity of 185 mAhg$^{-1}$ with high capacity retention over 40 cycles. A number of research work were carried out on fabricating anode material with combinations of $TiO_2$ with other metal oxides among which $TiO_2$-$SnO_2$ composite materials are commonly studied.[238-241] Another effective way to improvise the electrical conductivity of $TiO_2$ is by making $TiO_2$-C nanocomposites. Several research works are available on preparing $TiO_2$-C nanocomposites in different form of nanostructures.[37, 120, 121, 242, 243] Wang et al.[242] fabricated porous $TiO_2/C$ nanocomposite hollow shells by sol-gel method with high capacity of 288.2 mAhg$^{-1}$ at a current rate of 0.1C,

This journal is © The Royal Society of Chemistry 2014

*J. Mater. Chem*. A, 2014, **00**, 1-3 | **13**

excellent cycle stability over 300 cycles, and rate performance. Grafting of nanosized $TiO_2$ on graphene nanosheets is a straightforward way to increase electrical conductivity. Xin et al.[121] fabricated $TiO_2$-graphene nanocomposite by assembling hydroxyl titanium oxalate precursor in a flower-like structure with the help of surfactant followed by calcination. These nanocomposites delivered exceptionally high rate capability with a capacity of 230 mAhg$^{-1}$ at 0.1 C and excellent cycling stability. Lou and his co-workers fabricated the nanocomposite by growing ultrathin anatase $TiO_2$ nanosheets with exposed high-energy (001) facets onto graphene support for fast lithium storage showing the specific capacity value ~ 200 mAg/h at a current rate 0.1 C.[37] Wang et al.[120] developed both anatase as well as rutile $TiO_2$-graphene hybrid nanostructures by self-assembly of metal oxides and graphene via an anionic surfactant mediated growth. The nanocomposites showed a significant enhancement in the performance than the pristine materials. Symbiotic coaxial nanocables made of carbon nanotube as core and $TiO_2$ nanoporous sheath reported by Maier and his group showed high performance as anode electrode in LIB with the reversible capacity of 406 mAhg$^{-1}$ at a current rate 50 mAg$^{-1}$.[243] Though, $TiO_2$ shows greater cyclic stability, its extensive use is inhibited due to not so high specific capacity values. Considering the fact, Liao et al.[74] assembled core-shell nanowires with the combination of $MnO_2$, $TiO_2$ and C to design an effective anode for LIB utilizing the high specific capacity value of $MnO_2$, cyclic stability of $TiO_2$ and C-coating for electrical conductivity. The electrode was fabricated by hydrothermal method forming freestanding $TiO_2$/C core-shell nanowires on flexible Ti-foil followed by layer-by-layer deposition of $MnO_2$ nanoparticles. As per the anticipation, the electrode showed highly improved electrochemical performance between 0.01 and 3 V (vs. Li/Li$^+$) with specific capacity value ~ 350 mAhg$^{-1}$ at the current rate 1 C over 100 cycles.

Theoretical capacity values of manganese oxides ($MnO_x$) are high enough and vary depending on their different forms and phases of oxides, e.g., $MnO_2$ (1230 mAhg$^{-1}$), MnO (755 mAhg$^{-1}$) and $Mn_3O_4$ (936 mAhg$^{-1}$). However, extremely poor electrical conductivity and rapid capacity fading of $MnO_x$ due to volume expansion and aggregation in the discharge–charge process suppress the use of pristine $MnO_x$. The reports are mostly focused on synthesis of $MnO_x$-C nanocomposites for their application as anode in LIB.[129, 244] Cui and his group successfully synthesized $Mn_3O_4$ nanoparticles anchored on reduced graphene oxide (RGO) by a two-step solution-phase reaction.[130] By this approach the insulating nature of $Mn_3O_4$ nanoparticles was overcome by incorporating the oxide nanoparticles in to the RGO. This was also confirmed by more than 4-fold enhancement of reversible capacity of $Mn_3O_4$-RGO nanocomposite over free $Mn_3O_4$ nanoparticles with great cycle stability. The cell showed a stable specific capacity of 900 mAhg$^{-1}$ at a current rate of 40 mAg$^{-1}$ with Coulombic efficiency of 98%. An excellent cycle stability was observed for $Mn_3O_4$ nanorods dispersed on graphene nanosheet with the reversible capacity value of 100 Fg$^{-1}$ at the current rate 5 Ag$^{-1}$ over 10000 cycle with 100% retention.[54] In another approach, a hierarchical structure of graphene-wrapped $MnO_2$–graphene nanoribbons were fabricated by Lei et al.[129] Such complex structure was fabricated in two steps by hydrothermal method to synthesize $MnO_2$@graphene nanoribbon followed by chemical treatment and introducing into graphene solution for wrapping with graphene nanosheet. The electrode exhibited enhanced specific capacity of ~ 800 mAhg$^{-1}$ at a current rate of 0.4 Ag$^{-1}$ and

improved cycling stability up to 250 cycles as an anode material compared to $MnO_2$-graphene and pure $MnO_2$ because of the synergic effect between the graphene, graphene nanoribbons, and $MnO_2$. The electrode composed of $MnO_2$ nanoflakes coated on carbon nanohorns (CNHs) were also synthesized via a facile solution method where CNHs act as buffer carrier, resulting an excellent capacity of ~ 600 mAhg$^{-1}$ measured at a high current density of 100 mAg$^{-1}$ even after 60 cylces.[244] The free $MnO_2$ showed a significant capacity fading after 20 cycles indicating clearly the role of CNHs. In addition, different metal-based support has also been used to improve the electronic transportation. For example, interconnected porous MnO nanoflakes grown on Ni foam showed high reversible capacity up to 648.3 mAhg$^{-1}$ after 100 cycles at a current density of 246 mAg$^{-1}$.[77]

Different forms of iron oxides, such as, hematite ($\alpha$-$Fe_2O_3$), magnetite ($Fe_3O_4$) to ferrous oxide (FeO) have been extensively used in biological to industrial applications due to their availability and environmental benignity. Among them, $\alpha$-$Fe_2O_3$ is thermodynamically most stable oxide and used as a promising anode in LIB due to its high theoretical capacity value (1007 mAhg$^{-1}$). Tarascon and his co-workers studied fir the first time lithium intercalation in different nanosized $\alpha$-$Fe_2O_3$ particles.[245, 246] As per their observation, large particles (~ 0.5 µm) undertook only small amount of lithium ($Li_xFe_2O_3$, x < 0.1), whereas nanosized $\alpha$-$Fe_2O_3$ (20 nm) inserted up to one Li per formula unit ($Li_xFe_2O_3$, x = 1) without any phase transformation. Directly grown $Fe_2O_3$ nanostructures on to conductive substrates (Cu or Ti foil) are preferred due to their direct attachment to the current collector avoiding use of additives and thereby facilitating the electron collection efficiency.[247-249] Chowdari and his group[247] synthesized $\alpha$-$Fe_2O_3$ nanoflakes grown on Cu-foil by radio frequency (rf) magnetron sputtering. The electrode showed the stable capacity of ~ 700 mAhg$^{-1}$, with no noticeable capacity fading up to 80 cycles, in the range of 0.005–3.0 V at current rate of 65 mAg$^{-1}$ (0.1 C rate). The nanoflake structure of $\alpha$-$Fe_2O_3$ are found to be superior than nanoparticle or nanotubular forms as they showed noticeable capacity fading up to 50% after 15 cycles. A large arrays of $\alpha$-$Fe_2O_3$ nanotube layers, with enhanced electrochemical properties in LIB, were fabricated using anodic alumina as hard template or ZnO nanowires as sacrificial template.[249, 250] Chen et al.[251] synthesized single crystalline $\alpha$-$Fe_2O_3$ nanodisc by a top-down method and particles with tunable porosity by controlled etching. In this, phosphate ions acted as a capping agent to control the etching to along the (001) direction. The pore size as well as the surface area of $\alpha$-$Fe_2O_3$ microparticles was controlled by the etching time. The material exhibited a significantly improved capacity retention compared to the pristine one. Lou et al.[70] fabricated $\alpha$-$Fe_2O_3$ hollow spheres by hydrothermal conditions via interesting glycerol/water quasiemulsion-templating mechanism. This material, when used as anode material, accommodated the strain during lithium intercalation-deintercalation process and showed good performance with specific capacity near 900 mAhg$^{-1}$ at the current rate 200 mAg$^{-1}$ between 0.05 and 3 V. Koo and his co-workers[252] synthesized Fe/$Fe_3O_4$ core/shell nanoparticles by vacancy coalescence technique during oxidation. The technique involves an annealing process oxidizing $Fe_3O_4$ into $\gamma$-$Fe_2O_3$ hollow nanosphere creating cation vacancy. The vacant site in the hollow spheres a considerable increment in the specific capacity value above 1200 mAg/h in the voltage range 0.01-3.0 V. Liu et al.[253] fabricated fiber-like 1D macroporous $Fe_2O_3$ by in situ synthesis of $Fe_2O_3$

nanoparticles in the regenerated cellulose fibers during the wet spinning process, followed by the removal of cellulose matrix by calcination. The material showed excellent capacity value ~ 1200 mAhg$^{-1}$ with good capacity retention up to 50 cycles at a current density 100 mAg$^{-1}$. In order to improve the electrical conductivity, synthesis of reduced graphene oxide (RGO)/Fe$_2$O$_3$ nanocomposites was also reported in a two-step process of homogeneous precipitation of Fe$_2$O$_3$ nanoparticles on to GO followed by reduction of GO with hydrazine under microwave irradiation.[122] RGO, in their approach, provided a C-frame to improve the conductivity of the electrode and perform electrochemical analysis in the voltage range between 3.0 and 0.005 V vs Li$^+$/Li indicated 10.1 mol of Li uptake unit mole of Fe$_2$O$_3$. The cycling performance of RGO/Fe$_2$O$_3$ nanocomposite showed a specific capacity value of ~ 1100

mAhg$^{-1}$ at current density 100 mAg$^{-1}$ up to 50 cycles. This was found to be considerably stable compared to the physically mixed Fe$_2$O$_3$ nanoparticles and RGO in the same ratio. Fe$_2$O$_3$ nanorice or nanoparticles anchored on graphene nanosheets were prepared by microwave-assisted hydrothermal technique and showed a high reversible capacity of 1184 mAhg$^{-1}$ at 100 mAg$^{-1}$ up to 40 cycles.[127] Other most studied nanocomposites involved the combination of other metal oxides, e.g., Co$_3$O$_4$, SnO$_2$ or TiO$_2$ with Fe$_2$O$_3$ as hetero-nanostructures in the form of core-shell, branched structure etc.[71, 78, 254-257] Such hetero-nanostructured electrode found to be excellent candidate in LIB due to synergistic effect between $\alpha$-Fe$_2$O$_3$ and other metal oxides. The reduction in initial irreversible loss and high specific capacity is observed in the range of ~ 1000 mAhg$^{-1}$ at current density 100 mAg$^{-1}$.
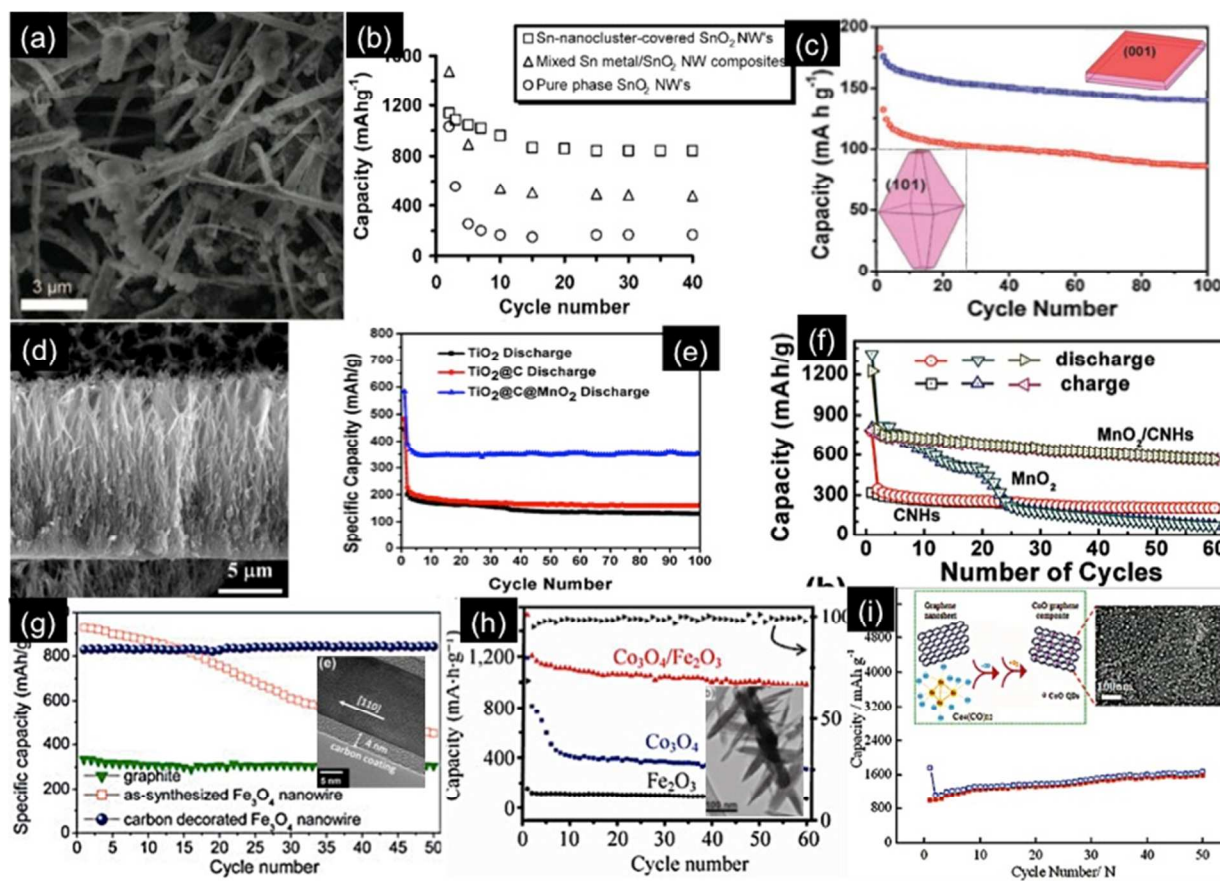


**Fig. 13**: Cyclic performance comparison of different nanodimensional transition metal oxides and their nanocomposites in LIB: (b) Sn-nanocluster-covered SnO$_2$ nanowires (SEM image in (a)), SnO$_2$ nanowires with dispersed Sn metal, and pure SnO$_2$ nanowires measured between 0 to 2.2 V (Reprinted with permission from ref 227. Copyright 2009 American Chemical Society); (c) anatase TiO$_2$ with dominant (001) (blue) and (101) (red) facets at current rate 10C (Ref 235); (e) bare TiO$_2$ and TiO$_2$-C, TiO$_2$-C/MnO$_2$ (SEM image in (d)) nanocomposites at a rate of 1 C (Reprinted with permission from ref 74. Copyright 2013 American Chemical Society); (f) carbon nanohorns (CNHs), MnO$_2$ and MnO$_2$/CNH electrodes at a current density of 100 mAg$^{-1}$ (Reprinted with permission from ref 243. Copyright 2012 American Chemical Society); (g) Fe$_3$O$_4$ nanowires before and after carbon decoration at 0.1C rate (*inset*: HRTEM image of crystalline Fe$_3$O$_4$ nanowires surrounded by amorphous carbon) (Ref 260); (h) Co$_3$O$_4$/$\alpha$-Fe$_2$O$_3$ branched NW, Co$_3$O$_4$ NW, and $\alpha$-Fe$_2$O$_3$ NW anodes at a current density of 100 mAg$^{-1}$ (*inset*: TEM image of Co$_3$O$_4$/$\alpha$-Fe$_2$O$_3$ branched NW) ((Reprinted with permission from ref 252. Copyright 2013 Springer); (i) CoO quantum dot/graphene nanocomposites at a current density of 50 m/g (*inset*: SEM image of nanocomposite) (Reprinted with permission from ref 117. Copyright 2012 American Chemical Society).

Magnetite (Fe$_3$O$_4$), consisting both Fe$^{2+}$ and Fe$^{3+}$, is also very promising candidate as anode material in LIB with the theoretical capacity value of ~ 900 mgA/h. In 2006, Tarascon et al.[258] reported the use of Fe$_3$O$_4$ as anode in LIB for the first time. Later on, the material was extensively studied by various research groups in the voltage range 0.01-3.0 V vs Li with good C-rate capability up to 8C.[9] Zhang et al.[126] fabricated Fe$_3$O$_4$

nanoparticle decorated on graphene nanosheet by *in situ* deposition of Fe$^{3+}$ and at the same time reducing graphene oxides with a microwave heater and a following thermal process. In this, the graphene nanosheet acted as a buffer layer in between Fe$_3$O$_4$ nanoparticles accommodating the strain generated during Li-insertion and removal process. The effect was clearly observed from their significantly enhanced cycling

This journal is © The Royal Society of Chemistry 2014

*J. Mater. Chem*. A, 2014, **00**, 1-3 | **15**

performances (about 650 mAhg$^{-1}$ after 50 cycles) and high rate capabilities (350 mAhg$^{-1}$ at 5 C). Li and his co-workers fabricated a 3D nannocomposite anode electrode for LIB anchoring Fe$_3$O$_4$ nanoparticles wrapped within carbon shells onto reduced graphene sheets and the electrode exhibited superior electrochemical properties with a specific capacity of 842.7 mAhg$^{-1}$ and superior recycle stability after 100 cycles.[123] Several other reports are available on Fe$_3$O$_4$-C nanocomposites and proved to be an outstanding anode electrode in LIB showing the specific capacity in the range of 900-1100 mAhg$^{-1}$ with good cyclability.[124, 125, 259-261] Synthesis of carbon coated 1D-Fe$_3$O$_4$ nanostructures (nanorods, nanowires and microbelts) were also attempted by several researchers as promising anode material in LIB. They exhibited the improved electrochemical properties due to their 1-D structures.[262-265] Moreover, hybrid Fe$_3$O$_4$@SnO$_2$ core–shell nanorod film directly grown on current collector is found to exert considerable areal capacitance (mF cm$^{-2}$ level) with long cycling stability up to 2000 cycles and thereby act as a supercapacitor as reported elsewhere.[266]

Cobalt-based oxides, CoO and Co$_3$O$_4$, are other suitable candidate as anode in LIB since the first report by Tarascon et al.[267] in 2000. Co$_3$O$_4$ is a mixed valent oxide with spinel structure containing both Co$^{2+}$ as well as Co$^{3+}$. It can uptake 8 mole of Li per mole of Co$_3$O$_4$ in a reversible reaction showing the theoretical capacity 890 mAhg$^{-1}$ in the voltage range 0.005-3.0 V vs Li. Various nanodimesional form of Co$_3$O$_4$ can be prepared by co-precipitation method, hydrothermal synthesis or using anodic alumina (AAO) as hard template.[268-270] Core-shell nanostructured Co$_3$O$_4$ found to be successful in accommodating strain during the Li-insertion-removal process as expected. Son et al.[271] fabricated yolk-shell Co$_3$O$_4$ powder with solid core and multiple shells by spray pyrolysis technique in different temperatures and found to be very stable even at a high discharge rate of 10,000 mAg$^{-1}$. A significant enhancement in the specific capacity value was observed for multishelled Co$_3$O$_4$ hollow spheres fabricated by a template-assisted growth.[272] The material showed an exceptionally high specific capacity above 1500 mAhg$^{-1}$ at a current rate of 50 mAg$^{-1}$ up to 30 cycles. Huang et al.[273] synthesized Co$_3$O$_4$ microcubes composed of nanoparticles by surfactant-assisted hydrothermal method from single crystal CoCO$_3$ microcube precursor and studied their performance as anode material in LIB. Such material with high surface area exhibit high initial discharge capacities (1298 mAhg$^{-1}$ at 0.1 C and 1041 mAhg$^{-1}$ at 1 C) with excellent capacity retention values over 90%. 1D-nanostructures of Co$_3$O$_4$ also found to be very promising to attain high specific capacity in the range of 700-900 mAg/h with good retention capability.[50, 274, 275] Free-standing CoO nanowires on to flexible conductive substrate are found to be even more promising for LIB due to the robust adhesion to the current collector and thereby good mechanical stability after several cycles.[50, 275] Synthesis of different nanocomposites of Co$_3$O$_4$ with carbonaceous materials, and other different metal oxides are also reported by several research groups.[72, 117, 118, 255, 269, 276, 277] Anchoring of Co$_3$O$_4$ or CoO nanoparticles on graphene nanosheet layers found to be fruitful approach for improving the electrical conductivity of material and accommodating strain during the intercalation-deintercalation process.[117, 118] While Co$_3$O$_4$/graphene nanocomposites with Co$_3$O$_4$ particle size 10-30 nm showed the reversible capacity value ~ 1000 mAhg$^{-1}$, smaller sized (~5 nm) CoO quantum dot/graphene nanocomposites exhibited outstanding reversible capacity value of 1600 mAhg$^{-1}$ at current density of 50 mAg$^{-1}$ stable up to 50 cycles. Qi et al.[269] fabricated Co$_3$O$_4$@SnO$_2$@C core-shell

nanorods via facile hydrothermal and subsequent carbonization process. The material found to be superior electrode due to an elegant synergistic effect of Co$_3$O$_4$ and SnO$_2$,[278] showing the stable reversible capacity value ~ 1000 mAhg$^{-1}$ at a current rate 200 mAg$^{-1}$ stable up to 50 cycles. The synergistic effect of bi-component nanocomposites, like, CoO/CoFe$_2$O$_4$, directly grown Co$_3$O$_4$/NiO nanorods on conductive substrate also found to be promising as anode electrode in LIB.[72, 277]

NiO, having the theoretical capacity 718 mAhg$^{-1}$, can be used as anode electrode in LIB as reported by Tarascon in 2000. It showed the initial reversible capacity of ~ 600 mAhg$^{-1}$, which slowly degraded to ~200 mAhg$^{-1}$ after 50 cycles in the voltage range of 0.01–3.0 V.[267] NiO, in different nanodimensional forms (nanoflakes, nanoparticles), synthesized by hydrothermal method or by controlled chemical synthesis process, and showed the reversible capacity value 500–600 mAhg$^{-1}$ at current rate 50 mAg$^{-1}$.[279-281] Sasidharan et al.[282] synthesized NiO hollow spheres of size 30 nm by a soft-template self-assembly process using poly(styrene-b-acrylic acid-b-ethylene oxide) as template. The hollow spheres when used as anode, delivered a capacity of 393 mAhg$^{-1}$ after 50 cycles of charge–discharge at a rate of 0.3 C and maintained the structural integrity with excellent cycling stability even after subjecting to a high rate of 10 C. It is believed that addition of metals with high density, like Au, Ag and Ni, contributes to the excellent electrochemical properties, in terms of electrical conductivity and cycle stability.[283-286] In addition, the formation of nanocomposites with carbon or other metal oxides are also another well-known approach in order to improve electrochemical properties.[73, 132, 287, 288] Such nanocomposites exhibited considerably high and stable specific capacities ~ 1000 mAhg$^{-1}$ at current density 50 mAg$^{-1}$.

Though ZnO nanostructures are mostly used as hard and sacrificial template, they can also be used for anode in LIB as sole materials or in the form of composites with metals as well as other metal oxides.[289-291] However, they have not been much explored due to their experimentally obtained low specific capacity values and lack of cyclic stability. A comparative study of cycling performance of different TMOs and their nanocomposites are represented in Fig. 13.

Mixed metal oxides or their hybrid materials with carbonaceous material are also considered to be effective anode material in LIB. CoSnO$_3$/Graphene nanohybrid materials were synthesized by solvothermal method followed by dispersion on the graphene nanosheets reduced from GO.[292] When the material was used as anode material, exhibited stable reversible capacity values even at very high current density (e.g. at 3200 mAg$^{-1}$ yields charge capacity of 248 mAhg$^{-1}$). Recently, much attention have also been paid on development of spinel structured ternary metal oxides of AB$_2$O$_4$ where A and B are two transition metals with the oxidation states +2 and +3, respectively.[293-298] Such compounds are able to store Li$^+$ ion through a series of possible conversion reactions (17-19) as well as alloy formation reactions (20-21):

$$AB_2O_4 + xLi^+ + xe^- \rightarrow A + B + Li_2O \qquad (17)$$
$$A + Li_2O \leftrightarrow AO + 2Li^+ + 2e^- \qquad (18)$$
$$B + Li_2O \leftrightarrow BO + 2Li^+ + 2e^- \qquad (19)$$
$$A + Li^+ + e^- \rightarrow LiA \qquad (20)$$
$$B + Li^+ + e^- \rightarrow LiB \qquad (21)$$
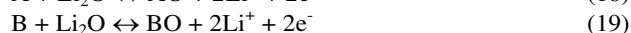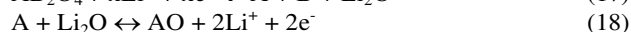
Spinel NiCo$_2$O$_4$ with different nanoarchitectures and their nanocomposites with C-based materials are extensively studied as anode electrode in LIB or in supercapacitor.[293-295] Zheng et

al.[294] fabricated 2D mesoporous $Ni_xCo_{3-x}O_4$ nano- sheets after the heat treatment of Ni-Co-hydroxide precursor. The porous and 2D textural structure provide huge surface area enhancing the electrolyte contact area, which is responsible for exhibiting outstanding performance as anode electrode in LIB. A reversible capacity of 1330 mAhg$^{-1}$ at a current density of 100 mAg$^{-1}$ after 50 cycles was obtained with 96.6% of capacity retention, which further reached stable reversible capacity of 844 mAhg$^{-1}$ at relatively high current density of 500 mAg$^{-1}$ after 200 cycles. Shakir et al.[293] fabricated $NiCo_2O_4$ anchored on the MWCNT and used them as electrode in the energy storage device. The composite electrode showed excellent performance with high specific capacitance of 2032 Fg$^{-1}$ in compared to 1235 Fg$^{-1}$ for pristine $NiCo_2O_4$ nanoflakes both at high current density of 1 Ag$^{-1}$ upto 5000 cycles. Very recently, Huang et al.[299] developed $NiFe_2O_4/Fe_2O_3$ nanotubes from metal organic frameworks under solvothermal treatment followed by annealing. The material showed considerably high specific capacity of 936.9 mAhg$^{-1}$ at a current density of 100 mAg$^{-1}$ up to 100 cycles. Spinel $ZnMn_2O_4$ nanocrystals anchored onto a

three dimensional (3D) porous carbon aerogel was prepared through a facile solution immersion chemical route.[296] Such interconnected porous C-matrix provide abundant porosity and high electron transport properties, which can be reflected from the high reversible capacity of 833 mAhg$^{-1}$ at a current density of 100 mAg$^{-1}$, even higher than the theoretical capacity of 784 mAhg$^{-1}$ for pure spinel $ZnMn_2O_4$ materials, with a Coulombic efficiency of 99.9%. The anisotropic, hollow and porous nanostructure of $Zn_xCo_{3-x}O_4$ are also found to be effective anode material in LIB with a reversible capacity value in the range of ~ 1000 mAhg$^{-1}$ (@ 1C) up to 50 cycles as reported by Ajayan and his co-workers.[297] Liu et al.[298] designed flexible anode electrode for LIB composed of hierarchical 3D $ZnCo_2O_4$ nanowire arrays on carbon cloth. The electrode exhibited outstanding performances in terms of capacity, rate capability, and cycle-life. The full battery set up composed of this 3D hybrid anode and $LiCoO_2$ cathode showed reversible capacity of > 1200 mAhg$^{-1}$ at current density 200 mAg$^{-1}$ stable up to 160 cycle with great capacity retention.

**Table 1**: Synthetic strategies and electrochemical properties of transition metal oxide based anode materials in lithium ion rechargeable batteries.

| # | Sample | Methods | Size | Sp. capacity (mAhg$^{-1}$) | Current Density | # cycles | % retention | Ref. |
|---|--------|---------|------|------------------|-----------------|----------|-------------|------|
| 1. | $SnO_2$ hollow nanostructures | Hydrothermal | 100-250 nm | 1140 | 0.2 C | 40 | -- | [227] |
| 2. | $SnO_2$ hollow nanoboxes | Template-engaged etching | 200 nm – 1 µm | 570 | 0.2 C | 40 | -- | [66] |
| 3. | Mesoporous $SnO_2$ microspheres | Hydrothermal | 3-15 nm | 370 | 1 Ag$^{-1}$ | 100 | -- | [226] |
| 4. | $SnO_2$ nanorods | Hydrothermal | Dia: 60 nm L: 670 nm | 580 | 0.1 C | 100 | -- | [229] |
| 5. | $SnO_2$ nanowires | Vapour – liquid – solid method | Dia: 40-50 nm L: 1 µm | > 700 | 782 mAg$^{-1}$ | 50 | -- | [48] |
| 6. | $SnO_2$@carbon hollow nanosphere | Hard template ($SiO_2$) and hydrothermal | 250 nm | > 460 | 0.8 C (1 C = 625 mAg$^{-1}$) | 100 | -- | [43] |
| 7. | Co metal coated $SnO_2$ nanoparticles | Wet-chemical route | 100-150 nm | 810 | 0.1 C (1C = 782 mAhg$^{-1}$) | 50 | -- | [35] |
| 8. | $SnO_2$ nanowire covered with Sn nanoparticle | Microwave chemical vapour deposition | Dia: 30-100 nm L: few µm | > 800 | 100 mAg$^{-1}$ | 100 | 99% | [228] |
| 9. | Nanosized Rutile $TiO_2$ | Chemical reflux process | Dia: 10 nm L:30-40 nm | 132 | 1 C | 90 | -- | [19] |
| 10. | Anatase $TiO_2$ Nanosheets | Solvothermal | ~ 1 µm (sphere) | 190 | 1 C | 100 | -- | [234] |
| 11. | Porous $TiO_2$/C nanocomposite shells | Sol-gel process | 200-300 nm | 288.2 | 0.1 C | 300 | >98% | [242] |
| 12. | $TiO_2$/graphene nanocomposite | Surfactant-assisted and calcination | 1-1.5 µm | 230 | 0.1 C or 17 mAg$^{-1}$ | 350 | >98% | [121] |
| 13. | Anatase and rutile $TiO_2$/graphene nanocomposite | Surfactant mediated growth | 5-6 nm | Anatase: 160 Rutile: 170 | 1 C | 100 | 98% | [120] |
| 14. | 1D Mesoporous $TiO_2N_x$ | Electrospinning process | Dia: 100-200 nm L: few µm | 185 | 0.1 C | 40 | -- | [237] |
| 15. | $TiO_2$@CNT nanocables | Hydrolysis of $Ti(OBu)_4$ | Dia:150nm L: few µm | 406 | 50 mAg$^{-1}$ | 100 | -- | [243] |
| 16. | Graphene-supported anatase $TiO_2$ nanosheets | Solvothermal | 3-10 nm (mesopores) | 161 | 1 C | 120 | 90% | [37] |
| 17. | $TiO_2$ nanotube @$SnO_2$ nanoflake | ALD and Hydrothermal | Dia:~50nm L: ~ 1 µm | 580 | 1.6 Ag$^{-1}$ | 50 | -- | [238] |
| 18. | Mesoporous $TiO_2$:$RuO_2$ nanocomposite | Wet-chemical route | 300 nm | 214 | C/5 (30C = 10.08 Ag$^{-1}$) | 20 | -- | [36] |
| 19. | NiO@$TiO_2$ nanopowders | Flame spray pyrolysis | 34 nm | ~ 1000 | 300 mAg$^{-1}$ | 80 | 108% | [288] |
| 20. | $TiO_2$−C/$MnO_2$ core−double-shell nanowire arrays | Hydrothermal and layer−by−layer deposition method | Dia: 80 nm L: 12 µm | 471 | 0.1 C (1C = 335 mAg$^{-1}$) | 100 | 93% | [74] |
| 21. | MnO nanoflakes on Ni foam | Hydrothermal | Thickness: 300 nm | 700 | 246 mAg-1 | 200 | -- | [77] |
| 22. | $Mn_3O_4$ nanorods on graphene sheet | Hydrothermal | Dia:5-30 nm L:100-1000 nm | 100 Fg$^{-1}$ | 5 Ag$^{-1}$ | 10000 | 100% | [54] |
| 23. | $Mn_3O_4$-graphene hybrid | Two-step solution-phase reactions | 10-20 nm ($Mn_3O_4$ NP) | 900 | 40 mAg$^{-1}$ | 10 | -- | [130] |
| 24. | $MnO_2$ nanoflakes @ carbon nanohorns | Facile solution method | Caterpillar morphology | ~ 600 | 100 mAg$^{-1}$ | 60 | -- | [244] |
| 25. | Graphene-wrapped $MnO_2$–graphene nanoribbons | Hydrothermal | Dia: 200 nm | 612 | 0.4 Ag$^{-1}$ | 250 | 100% | [129] |
| 26. | α-$Fe_2O_3$ Hollow Spheres | Quasiemulsion-template | 1 µm | 750 | 200 mAg$^{-1}$ | 100 | 90% | [70] |

This journal is © The Royal Society of Chemistry 2014

*J. Mater. Chem.* A, 2014, **00**, 1-3 | **17**

| | | | | | | | | |
|---|---|---|---|---|---|---|---|---|
| 27. | $\alpha$-Fe$_2$O$_3$ nanoflakes | radio frequency (rf) magnetron sputtering | Thickness: 700 nm | ~ 700 | 65 mAg$^{-1}$ | 80 | >98% | 247 |
| 28. | Fiberlike Fe$_2$O$_3$ macro-porous nanostructure | Cellulose as template and calcination | Dia: 7.5 $\mu$m L: several 100$\mu$m | 1200 | 100 | 20 | -- | 253 |
| 29. | Mesoporous $\alpha$-Fe$_2$O$_3$ and Fe$_3$O$_4$ nanorods | Hydrothermal | Dia: 20-80 nm L: 400-700 nm | 1000 | 0.1 C (1C = 905 mAg$^{-1}$) | 50 | 92% | 55 |
| 30. | $\alpha$-Fe$_2$O$_3$ andFe$_3$O$_4$ Nanotube arrays | ZnO nanorods as sacrificial template-accelerated hydrolysis | Dia: 200 nm | 659 (C-coated), 384 (without coating) | C/5, (1C = 671 mA/g) | 150 | -- | 249 |
| 31. | Fe$_3$O$_4$ nanoparticle anchored on graphene | Microwave Irradiation | Dia: 20-70 nm | 650 | 0.1 C | 50 | -- | 126 |
| 32. | Fe$_3$O$_4$–Carbon–rGO nanocomposite | Hydrothermal | Dia: 10-20 nm | 843 | 0.2 C | 100 | >95% | 123 |
| 33. | Fe$_3$O$_4$–graphene nanocomposites | Ultrasonic assisted co-precipitation | Dia: 10 nm | 1200 | 2 C | 1000 | 96% | 124 |
| 34. | Fe$_3$O$_4$–carbon nanocomposites | Hydrothermal | Dia: 10 nm | 1249 | 0.1 C | 100 | 100% | 259 |
| 35. | Carbon-Encapsulated Fe$_3$O$_4$ Nanoparticles | Facile and scalable in situ synthesis method | Dia: 5-25 nm | 858 | 5 C (1 C = 1 Ag$^{-1}$) | 350 | 96% | 260 |
| 36. | Fe$_2$O$_3$-graphene rice-on-sheet nanocomposite | Microwave-assisted hydrothermal technique | Particle: 50-80 nm Rice: 150-200 nm | 1184 | 100 | 40 | -- | 127 |
| 37. | Reduced graphene oxide /Fe$_2$O$_3$ nanocomposite | Precitation reaction and microwave irradiation | Dia: 60 nm | ~ 1100 | 100 | 50 | -- | 122 |
| 38. | FeO$_x$□Coated SnO$_2$ nanoparticle | Simple Solution Method | 10 nm | 480 | 400 mAg$^{-1}$ | 150 | -- | 257 |
| 39. | $\alpha$-Fe$_2$O$_3$@SnO$_2$ nanorattles | Hydrothermal | 450 nm | 419 | 200 mAg$^{-1}$ | 30 | -- | 71 |
| 40. | Fe$_3$O$_4$@Carbon Nanorods | Glucose-mediated hydrothermal method | Dia: 20-50 nm L: 50-200 nm | 800 | 924 | 100 | -- | 262 |
| 41. | Carbon-decorated single-crystalline Fe$_3$O$_4$ nanowire | Microwave-hydrothermal approach | Dia: 20-50 nm L: several $\mu$m | 830 | 0.1 C | 50 | 100% | 263 |
| 42. | Branched Co$_3$O$_4$/Fe$_2$O$_3$ nanowires | Hydrothermal | Dia: 70 nm (Co$_3$O$_4$) Dia: 40 nm (Fe$_2$O$_3$) Thickness: 5 $\mu$m | 1000 | 100 | 60 | -- | 255 |
| 43. | Branched $\alpha$-Fe$_2$O$_3$/SnO$_2$ nano heterostructures | Vapour transport deposition and hydrothermal | Dia: 50 nm L: 500 nm (sub-nanorods) | 1167 | 1000 mAg$^{-1}$ | 30 | 50% | 78 |
| 44. | Co$_3$O$_4$ yolk-shell powder | Spray pyrolysis | 1 $\mu$m | 750 | 1400 | 100 | -- | 271 |
| 45. | Multishelled Co$_3$O$_4$ hollow microspheres | Template-assisted growth | 1 $\mu$m | 1600 | 50 | 30 | 100% | 272 |
| 46. | Co$_3$O$_4$ microcubes consisting nanoparticles | Surfactant-assisted hydrothermal | 2-3 $\mu$m | 1298 1041 | 0.1 C 1 C | 60 | 99.3% 89.9% | 273 |
| 47. | Mesoporous Co$_3$O$_4$ nanowire arrays | Ammonia-evaporation-induced method | Dia: 500 nm L: 15 $\mu$m | 700 | 1 C | 50 | 50% | 50 |
| 48. | CoO Porous Nanowire Arrays | Hydrothermal and pyrolysis | Dia: 100 nm L: 2 $\mu$m | 670 | 1C | 20 | -- | 275 |
| 49. | Co$_3$O$_4$ Nanotubes | Topotactic transformation | Dia:150-400 nm L: 10 $\mu$m | 900 | 50 | 30 | 100% | 274 |
| 50. | Co$_3$O$_4$ nanoparticles anchored on graphene | Chemical exfoliation and calcination | 10-30 nm | 1000 | 50 | 30 | 100% | 117 |
| 51. | CoO Quantum dot/ graphene nanocomposites | Ultrasonic method | ~ 5 nm | 1600 | 50 | 50 | 100% | 118 |
| 52. | SnO$_2$@silica double shell hollow sphere Co$_3$O$_4$@SnO$_2$@C | Thermal treatment | 400 nm | 800 | 160 mAg$^{-1}$ | 50 | -- | 68 |
| 53. | Co$_3$O$_4$@SnO$_2$@C core-shell nanorods | Hydrothermal and Carbonization | Dia: 30 nm | 1000 | 200 | 50 | 100% | 269 |
| 54. | NiO nanoplates | Hydrothermal | 90-120 nm | 500 | 50 | 20 | -- | 279 |
| 55. | NiO nanoflakes | Controlled Chemical Synthesis | 50-100 nm | 410 | 50 | 40 | 98% | 280 |
| 56. | NiO hollow spheres | Soft-template self-assembly process | Dia: 30 nm | ~ 400 | 0.3 C | 50 | -- | 282 |
| 57. | 3D macroporous NiO/Ni powder | Metal Complex Chemical Route | Flakes: 1-2 $\mu$m Thickness: 10 nm | ~ 700 | 1 C | 50 | 100% | 281 |
| 58. | NiO-coated ZnO nanorod arrays | Hard template (ZnO)assisted growth | Dia: 60-120 nm | ~ 1100 | 1 C | 15 | 97% | 73 |
| 59. | Co$_3$O$_4$/NiO and ZnO/NiO core/shell nanowire array | Hydrothermal | Dia: 70 nm L: 10 $\mu$m | 853 Fg$^{-1}$ | 1 Ag$^{-1}$ | 6000 | 95% | 72 |
| 60. | 2D mesoporous Ni$_x$Co$_{3-x}$O$_4$ nanosheets | Thermal Decomposition | Dia: 2 $\mu$m Thickness: 2 nm | 1330 844 | 100 mAg$^{-1}$ 500 mAg$^{-1}$ | 50 200 | 96.6% -- | 294 |
| 61. | Hollow and porous nanostructure of Zn$_x$Co$_{3-x}$O$_4$ | Template-assisted Co-precipitation method | ~ 1 $\mu$m | ~ 1000 | 1 C | 50 | -- | 297 |
| 62. | Hierarchical 3D ZnCo$_2$O$_4$ nanowire arrays on carbon cloth | Solvothermal | Dia: 80-100 nm (NW) L:5$\mu$m (NW) Dia: 20 $\mu$m (C fiber) | > 1200 | 100 mAg$^{-1}$ | 160 | 99% | 298 |
| 63. | ZnMn$_2$O$_4$ nanocrystals anchored on 3D porous carbon aerogel | Solution immersion chemical route | 40 nm | 833 | 100 mAg$^{-1}$ | 60 | 50.3% (>96% after 5 cylces) | 296 |

Journal of Materials Chemistry A Accepted Manuscript

| 64. | CoO/CoFe$_2$O$_4$ nanocomposites | Calcination | | 100 nm | 1000 | 100 | 100 | 98% | [277] |

## 4.6 Layered Metal Dichalcogenides and their Composites

Layered metal dichalcogenides (MX$_2$) exhibit excellent lithium ion storage capacity due to their special layered arrangement in crystal structures. In MX$_2$, the metal atoms are sandwiched in between two hexagonally arranged chalcogenide layers in the form of X–M–X, which are attached with another unit through weak van der Waal's forces. Such layered stacking arrangement provide enough space for the lithium intercalation in the tetrahedral or octahedral interstitial sites, where later is energetically more favoured.[82, 300] Moreover, the lithium intercalation in MX$_2$ involves a complete charge transfer reducing M$^{4+}$ to M$^{3+}$ ion along with Li$^+$ ion diffusion in the van der Waal's gap resulting volume expansion.[82] Depending upon the lithiation potential values, metal sulfides MS$_2$ of M = Fe, Ti, Co, Ni, and Cu are considered as cathode material, whereas M = Mo, W, Ga, Nb, and Ta are known to be used as anode material in LIB.[92]

Molybdenum disulfides undergo lithiation at relatively high potential value ~ 2V and used as anode while paired up with high voltage lithiated cathode (say ~ 4 V). The theoretical capacity value for MoS$_2$ is > 670 mAhg$^{-1}$ accommodating 4 mole of Li$^+$ ion per unit according to the following electrochemical reaction:

$$MoS_2 + 4Li^+ + e^- \leftrightarrow Mo + 2Li_2S \qquad (22)$$

However, Li$_2$S, formed during the reaction, is very reactive with electrolye forming the SEI on the surface of the electrode material affecting the cyclic stability and rate capability. Recent studies show that nanocomposites of MoS$_2$ with carbonaceous material are considered to be another promising material with the reversible capacity value in the range of 900-1000 mAhg$^{-1}$ and good cyclic stability.[97, 301-304] Yang et al.[305] reported a stable reversible capacity of 902 mAhg$^{-1}$ at 100 mAg$^{-1}$ up to 80 cycles, fabricating hierarchical hollow nanoparticles of MoS$_2$ nanosheets with an increased interlayer distance by simple solvothermal method. Archer and his group prepared composite material of MoS$_2$ with amorphous carbon via hydrothermal method.[301] Such MoS$_2$-C nanocomposite electrode with 22% of carbon content showed best performance with a stable reversible capacity value ~ 900 mAhg$^{-1}$ as the thick carbon coating onto MoS$_2$ inhibit direct contact of Li$_2$S with the electrolyte increasing the electrode stability. An excellent stability in discharge capacity can be attained by making composite of ultrathin MoS$_2$ nanosheets with graphene as reported by Zhang et al.[303] MoS$_2$ with 2D nanowall also provide a better electrochemical performance and stability when combined with cellulose binder.[302] Sen and Mitra synthesized such electrode material by a two-step chemical synthesis method and it showed a stable capacity of 880 mAhg$^{-1}$ at a current rate of 100 mAg$^{-1}$. Srivastava and his co-workers prepared the MoS$_2$–MWCNT hybrid materials by simple grinding technique.[97] The electrochemical performance of such electrode showed an exceptionally high and stable capacity value in the range of 1100-1200 mAhg$^{-1}$ up to 30 cycles. Such electrochemical behavior is attributed due to the synergistic effect of MWCNT and MoS$_2$ as well as surface defects generated during the grinding process, enhancing the lithium intercalation capacity.
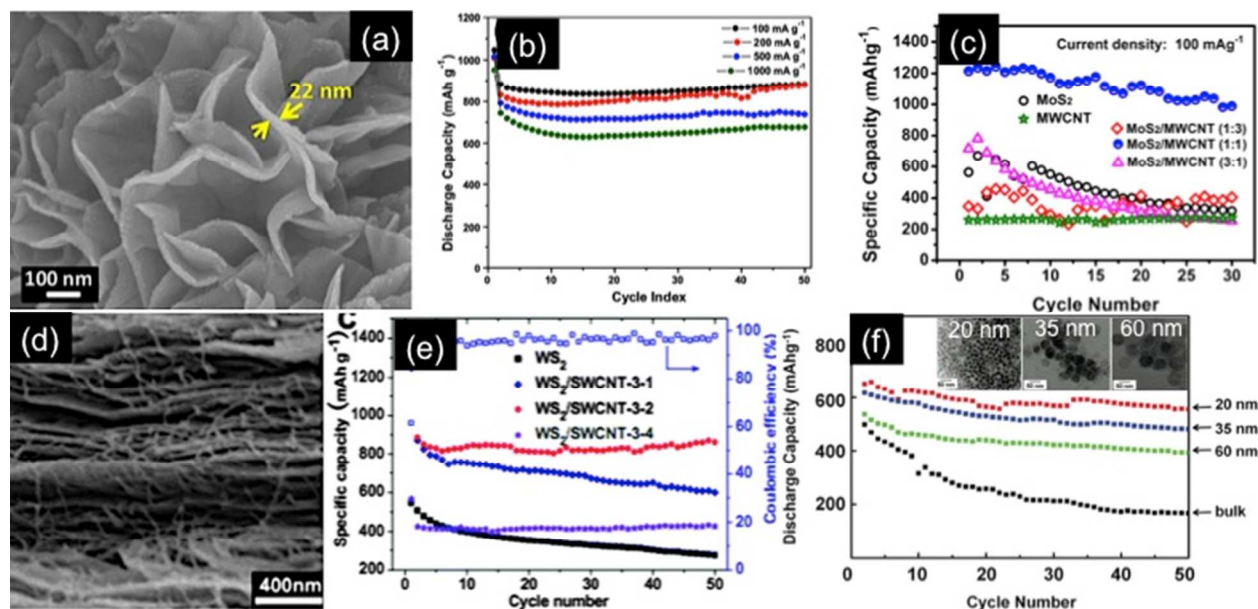


Fig.14: (a) SEM image of 2D MoS$_2$ nanowall and (b) their cyclic performance in presence of cellulose as binder at different current rates. Reprinted with permission from ref 294. Copyright 2013 American Chemical Society. (c) Cyclic performance of MoS$_2$:MWCNT hybrid materials in different ratios (Ref 96). (d) Cross-sectional SEM image of WS$_2$–SWCNT (3:2) hybrid film and (e) Cycling performance of WS$_2$–SWCNT hybrid films in different ratios at current rate of 0.1 Ag$^{-1}$ (Ref 302). (f) Nanosize effect of ultrathin ZrS$_2$ on the discharge capacity in compared to bulk ZrS$_2$ at current rate 69 mAg$^{-1}$ (inset: TEM images of ultrathin-ZrS$_2$ nanodiscs with different lateral sizes). Reprinted with permission from ref 306. Copyright 2011 American Chemical Society.

Tungsten disulfide (WS$_2$) is another interesting layered type material from the transition meta dichalcogenide family. When used as anode material, it shows the theoretical capacity value of 433 mAhg$^{-1}$ allowing 4 mole of Li$^+$ ion per mole of WS$_2$

This journal is © The Royal Society of Chemistry 2014

J. Mater. Chem. A, 2014, 00, 1-3 | 19

forming $Li_xWS_2$ intercalated compound.[92, 306] Moreover, the morphology of material also plays very important role to decide $Li^+$ ion insertion capacity based on the available sites for intercalation showing higher reversible capacity values. Wang et al.[307] synthesized $WS_2$ nanotubes by sintering amorphous $WS_3$ at high temperature under flowing hydrogen and the nanotubular structure showed excellent electrochemical properties allowing easy $Li^+$ ion intercalation through open ends into the 4.6 nm diameter inner core as well as into intertubular sites. The $WS_2$ nanotube layers exhibited an initial high capacity value of ~900 mAhg$^{-1}$ which decreased to static 600 mAhg$^{-1}$ after 1$^{st}$ cycle. Such electrochemical behavior is attributed due to the trapping of a fraction of $Li^+$ ion inside the intertubular sites or caused by the decomposition of electrolytes on the $WS_2$ surface. Liu et al.[308] fabricated ordered mesoporous $WS_2$ with very high surface area and narrow pore size distribution by a vacuum assisted impregnation route. They noted that the material showed a high lithium storage capacity of 805 mAhg$^{-1}$ at a current of 0.1 Ag$^{-1}$ with high rate capability in compared to its bulk. Fang et al.[309] reported graphene-like $WS_2$ prepared by solid-state reaction of tungsten and sulfur powder and exhibited the reversible capacity value of 600 mAhg$^{-1}$ up to 100 cycles. Like $MoS_2$, composites of $WS_2$ with carbonaceous materials are revealed to be promising material achieving high as well as stable capacity values due to the synergistic effect of $WS_2$ and C.[310-312] Rao and his co-workers employed to synthesize $WS_2$ nanosheet supported on reduced graphene oxide (RGO) through a hydrothermal synthesis route.[311] The $WS_2$-RGO composite system delivered a reversible capacity value in the range of 400-450 mAhg$^{-1}$ over 50 cycles with good cyclability. Very recently, $WS_2$–SWCNT lamellar porous hybrid electrodes are fabricated by vacuum filtration as reported by Liu et al.[308] A very high capacity value of 1337.7 mAhg$^{-1}$ was observed, which decreased to 821.5 mAhg$^{-1}$ after 1$^{st}$ cycle due to SEI layer formation at the interface.

Among other transition metal chalcogenides, $SnSe_2$, $ZrS_2$, $TiS_2$ and their hybrid materials with carbonaceous materials are also found to be very promising in the field of anode materials used in LIB.[313-315] Ultrathin $ZrS_2$ nanodiscs were prepared by surfactant-assisted chemical synthesis process and proved to be a highly functional host material for the lithium intercalation process as reported by Jang et al.[314] Different sizes $ZrS_2$ nanodiscs of diameter 20, 35 and 60 nm with thickness of 1.6 nm acquire very high surface area and showed excellent nanoscale size effects, enhancing the discharge capacity by 230% and stability for 20 nm nanodiscs in comparison with bulk $ZrS_2$. $TiS_2$, having the layered structure like $MoS_2$, can also serve as a good host material for lithium intercalation forming $Li_xTiS_2$ (x = 0.12, 0.52, and 1.0) as intercalated compound.[316-318] Due to relatively high discharge capacity value of 2.1 V, $TiS_2$ is used mostly as cathode material rather than anode material in LIB. However, few reports are available where it is used as effective anode material in the form of hybrid material with carbonaceous material.[315]

**Table 2**: Synthetic strategies and electrochemical properties of transition metal dichalcogenide based anode materials in lithium ion rechargeable batteries.

| # | Sample | Methods | Size | Sp. capacity (mAhg$^{-1}$) | Current Density | # cycles | % retention | Ref. |
|---|--------|---------|------|----------------|-----------------|----------|-------------|------|
| 1. | Hierarchical hollow $MoS_2$ nanoparticles | Solvothermal | 300-800 nm | 902 | 100 mAg$^{-1}$ | 80 | -- | [305] |
| 2. | Ultrathin $MoS_2$ nanosheet-graphene nanocomposites | Hydrothermal | Interlayer spacing 0.62 nm | ~ 900 | 0.2 C (1C = 832 mAg$^{-1}$) | 50 | -- | [303] |
| 3. | 2D $MoS_2$ Nanowall and Cellulose Binder | Two-step Chemical Synthesis | Wall thickness: 22 nm | 880 | 100 mAg$^{-1}$ | 50 | 84% | [302] |
| 4. | $MoS_2$–MWCNT hybrid Materials | Grinding technique | -- | > 1100 | 100 mAg$^{-1}$ | 30 | 85% | [97] |
| 5. | $WS_2$ nanotubes | Sintering Method | Inner hollow core:4.6 nm | 600 | | 20 | -- | [307] |
| 6. | Ordered mesoporous $WS_2$ | Vacuum Assisted Impregnation | Pore size: 3-4 nm | 805 | 0.1 Ag$^{-1}$ | 100 | 98% | [308] |
| 7. | Graphene-like $WS_2$ | Solid-State Reaction | Thickness: 5.43 nm | 600 | 0.05 C (1C = 432 mAg$^{-1}$) | 100 | -- | [309] |
| 8. | $WS_2$–SWCNT lamellar porous nanocomposite | Vacuum Filtration | -- | 821 | 100 mAg$^{-1}$ | 50 | -- | [310] |
| 9. | $WS_2$ supported on reduced graphene oxide | Hydrothermal | -- | 400-450 | 100 mAg$^{-1}$ | 50 | -- | [311] |
| 10. | $WS_2$-MWCNT hybrid material | Grinding Method | -- | ~ 400 | 100 mAg$^{-1}$ | 20 | 80% | [312] |
| 11. | Ultrathin $ZrS_2$ nanodiscs | Surfactant-assisted Chemical Synthesis | Dia: 20, 35, 60 nm Thickness: 1.6 nm | 600 | 69 mAg$^{-1}$ | 50 | 86% | [314] |
| 12. | $TiS_2$–MWCNT hybrid materials | Grinding Method | -- | 340 | 100 mAg$^{-1}$ | 20 | 80% | [315] |

## Summery and Future Perspective

Lithium ion batteries with high energy and power density have become important for consumer electronic devices, portable power tools, and vehicle electrification. Miniaturization of electrodes in LIBs is the smart approach to store as much as possible energy in a small volume to address this huge energy demand. Till date, an enormous amount of research works has been reported in achieving high performance LIBs involving several approaches. Nanostructured anode materials provide a better efficacy about the fast Li intercalation/de-intercalation reactions, short $Li^+$ diffusion path length and fast electron transportation to the current collector. Therefore, the present article aims to provide an extended review on recent developments in LIB based on 0D, 1D and 2D nanostructured anode materials. Though earlier investigations were mostly focused on using single materials, now-a-days combinations of two or three materials as hybrids are investigated confronting the issues, like, specific capacity values; volume contraction or mechanical stability and capacity fading over cycles etc. In this regard, not only the choice of materials, but proper designing of

nanostructured hybrid materials is also very important to achieve desired properties of materials. The shape of nanostructure plays a very important role on the charge transportation kinetics affecting the LIB performances. It is attributed that 1D nanostructures are invariably superior to the 0D nanostructures allowing the fast directional electron transportation through the nanostructure to the current collector. Moreover, it is believed that the 1D nanostructures are able to accommodate the strain generated during the repeated Li$^+$ intercalation/de-intercalation process. The issues, like, volume expansion and the structural dis-integrity during the cycles can also be managed by core-shell or hollow nanostructured anode providing enough space for expansion-contraction during the lithiation-delithiation process. Another advanced approach is the fabrication of 3D branched heteronanostructures composed of more than one component. However, the complexity in designing such nanoarchitectures, composition uniformity, presence of defects, electronic transportation mechanism keeps the strategy still far from the requirement.

Till now, a number of materials have been attempted as promising anode materials in LIBs. Carbon-based materials with their versatility in structure, surface area and electrical conductivity, were the primary choice as anode in LIBs. However, significant capacity fading with cycles due to rigorous chemical reactions with electrolytes and SEI formation limits their use. Moderate results were obtained using spinel structured $Li_4Ti_5O_{12}$ in different forms of nanostructures. Further improvement in their capacity retention values were achieved by effective carbon coating on the $Li_4Ti_5O_{12}$ nanostructures. The concept of binary metal alloys turned out to be another interesting approach to design the anode for LIBs. The combination of metals in such binary alloys could be electrochemically either active-active or active-inactive in nature. While the first case involves the formation of various intermetallic or ternary alloy phases, the electrochemically inactive material in the second case act like a buffer against the volume expansion during lithiation process. Though reasonable results were attained by this approach, the complicated Li$^+$ intercalation/de-intercalation mechanism and irreversible nature of reaction steps during the cycles discourages their further use. Silicon, as an electrochemically active material, is the latest material of interest for anode having reasonably high theoretical capacity value. However, large volume changes during the lithiation-delithiation process resulting the capacity fading found to be big challenge for the researcher. Recently, the concept of conductive polymer coating on to the nanostructured Si have been proposed, which is likely to be fruitful way to resist the large volume change and structure damage during lithiation process.[319-321] A considerable amount of research was also focused on the transition metal oxides involving thermodynamically favourable reversible reaction with Li$^+$ ion, leading to good cyclability. However, poor electrical conductivity and low diffusion coefficient still exists as limiting factors. Some excellent results were also obtained from the transition metal dichalcogenides as anode with their special layered-type of structures facilitating Li intercalation-deintercalation process. Addition of carbon nanotubes and graphene into layered transitional metal dichalcogenides or metal oxides enhances the lithium uptake capacity further as revealed by superior specific capacity of the hybrids compared to their individual components. The approach not only provide the much needed mechanical stability, but also improve the electrical conductivity of the system.

Overall, it can be concluded that though significant progress has been made till now using different types of materials as anode in LIBs, performance-wise they are still far from the requirement. In order to overcome the limitations, like, low specific capacity (experimental) in compare to theoretical values, unusual volume expansion, irreversible reaction of Li$^+$ insertion/removal process, SEI layer formation, poor electrical conductivity etc., proper designing of nanostructures as well as combination of suitable materials are of great challenge, now-a-days. While the size, shape and designing of novel nanoarchitectures are important, rigorous side reactions due to very large surface area need to be avoided. Consequently, the electrode-electrolyte interface reaction mechanism should be properly examined. Furthermore, safety issues, non-toxic nature and low-cost materials should also be considered for commercial applications. In order to address this, electrodes composed of eco-friendly organic compounds or the organic/inorganic hybrid materials are believed to be promising.[322, 323] Another interesting approach to fabricate thin, flexible, bendable and stretchable energy storage devices based on textiles, plastics or papers loaded with CNTs or different metal oxides by 'dipping and drying' process or by printing have also been proposed.[324-329] Such simple and cheap devices are assumed to be useful to meet the high-energy demand in our modern society. However, all these techniques are now under development and further studies are required to understand the mechanism and accordingly the modifications need to be planned to improve their performance.

It is anticipated that the present review paper delivers an overview on recent scientific research and developments on nanostructured anode materials and could provide the insight of future development of high-performing anode materials in LIBs.

## Notes and references

1. J. M. Tarascon and M. Armand, *Nature*, 2001, **414**, 359-367.
2. B. Dunn, H. Kamath and J.-M. Tarascon, *Science*, 2011, **334**, 928.
3. *Brunswick, OH Pat.*, 1990.
4. B. Scrosati, *Nature*, 1995, **373**, 557.
5. R. F. Nelson, *J. Power Sources*, 2000, **91**, 2.
6. C. Jiang, E. Hosono and H. Zhou, *Nanotoday*, 2006, **1**, 28.
7. J. Tellefson, *Nature*, 2008, **456**, 436.
8. B. Scrosati and J. Garche, *Journal of Power Sources*, 2010, **195**, 2419-2430.
9. M. V. Reddy, G. V. S. Rao and B. V. R. Chowdari, *Chem Rev*, 2013, **113**, 5364-5457.
10. R. A. Huggins, *Advanced Batteries*, Springer Science+Business Media, New York, USA, 2009.
11. J. B. Goodenough, *Accounts Chem Res*, 2013, **46**, 1053-1061.
12. D. Liu and G. Cao, *Energy Environ. Sci.*, 2010, **3**, 1218-1237.
13. K. Xu, *Chem Rev*, 2004, **104**, 4303-4417.
14. J. Marcicki, A. T. Conlisk and G. Rizzoni, *Journal of Power Sources*, 2014, **251**, 157-169.
15. Z. Li, J. Huang, B. Y. Liaw, V. Metzler and J. B. Zhang, *Journal of Power Sources*, 2014, **254**, 168-182.
16. B. K. Purushothaman and U. Landau, *J Electrochem Soc*, 2006, **153**, A533-A542.
17. P. G. Bruce, B. Scrosati and J.-M. Tarascon, *Angew. Chem. Int. Ed.*, 2008, **47**, 2930.

18. Y. G. Wang, H. Q. Li, P. He, E. Hosono and H. S. Zhou, *Nanoscale*, 2010, **2**, 1294-1305.

19. Y. S. Hu, L. Kienle, Y. G. Guo and J. Maier, *Adv Mater*, 2006, **18**, 1421-1426.

20. A. S. Arico, P. Bruce, B. Scrosati, J. M. Tarascon and W. Van Schalkwijk, *Nat Mater*, 2005, **4**, 366-377.

21. M. J. Armstrong, C. O'Dwyer, W. J. Macklin and J. D. Holmes, *Nano Res*, 2014, **7**, 1-62.

22. S. Goriparti, E. Miele, F. De Angelis, E. Di Fabrizio, R. P. Zaccaria and C. Capiglia, *Journal of Power Sources*, 2014, **257**, 421-443.

23. Y.-G. Guo, J.-S. Hu and L.-J. Wan, *Adv Mater*, 2008, **20**, 2878-2887.

24. M.-Y. Cheng, Y.-S. Ye, T.-M. Chiu, C.-J. Pan and B.-J. Hwang, *J. Power Sources*, 2014, **253**, 27-34.

25. C. Wang, Q. Li, F. Wang, G. Xia, R. Liu, D. Li, N. Li, J. S. Spendelow and G. Wu, *ACS Appl. Mater. Interfaces*, 2014, **6**, 1243.

26. H. Q. Li and H. S. Zhou, *Chem Commun*, 2012, **48**, 1201-1217.

27. L. J. Fu, H. Liu, C. Li, Y. P. Wu, E. Rahm, R. Holze and H. Q. Wu, *Solid State Sci*, 2006, **8**, 113-128.

28. P. Yu, J. A. Ritter, R. E. White and B. N. Popov, *J. Electrochem. Soc.*, 2000, **147**, 1280.

29. P. Yu, J. A. Ritter, R. E. White and B. N. Popov, *J. Electrochem. Soc.*, 2000, **147**, 2081.

30. L. Shi, Q. Wang, H. Li, Z. Wang, X. Huang and L. Chen, *J. Power Sources* 2001, **102**, 60.

31. F. Nobili, S. Dsoke, M. Mancini and R. Marassi, *Fuel Cells*, 2009, **9**, 264-268.

32. H. Momose, H. Honbo, S. Takeuchi, K. Nishimura, T. Horiba, Y. Muranaka and Y. Kozono, *J. Power Sources*, 1997, **68**, 208.

33. K. Nishimura, H. Honbo, S. Takeuchi, T. Horiba, M. Oda, M. Koseki, Y. Muranaka, Y. Kozono and H. Miyadaera, *J. Power Sources*, 1997, **68**, 436.

34. S. S. Kim, Y. Kadoma, H. Ikuta, Y. Uchimoto and M. Wakihara, *Electrochem Solid St*, 2001, **4**, A109-A112.

35. L. Mei, C. C. Li, B. H. Qu, M. Zhang, C. Xu, D. N. Lei, Y. J. Chen, Z. Xu, L. B. Chen, Q. H. Li and T. H. Wang, *Nanoscale*, 2012, **4**, 5731-5737.

36. Y. G. Guo, Y. S. Hu, W. Sigle and J. Maier, *Adv Mater*, 2007, **19**, 2087-2091.

37. S. J. Ding, J. S. Chen, D. Y. Luan, F. Y. C. Boey, S. Madhavi and X. W. Lou, *Chem Commun*, 2011, **47**, 5780-5782.

38. N. Zhu, W. Liu, M. Q. Xue, Z. A. Xie, D. Zhao, M. N. Zhang, J. T. Chen and T. B. Cao, *Electrochim Acta*, 2010, **55**, 5813-5818.

39. L. Zhao, Y. S. Hu, H. Li, Z. X. Wang and L. Q. Chen, *Adv Mater*, 2011, **23**, 1385-1388.

40. H. G. Jung, J. Kim, B. Scrosati and Y. K. Sun, *Journal of Power Sources*, 2011, **196**, 7763-7766.

41. H. G. Jung, S. T. Myung, C. S. Yoon, S. B. Son, K. H. Oh, K. Amine, B. Scrosati and Y. K. Sun, *Energ Environ Sci*, 2011, **4**, 1345-1351.

42. K. T. Lee, Y. S. Jung and S. M. Oh, *J Am Chem Soc*, 2003, **125**, 5652-5653.

43. X. W. Lou, C. M. Li and L. A. Archer, *Adv Mater*, 2009, **21**, 2536-2539.

44. S. Kuwabata, N. Tsumura, S. Goda, C. R. Martin and H. Yoneyama, *J. Electrochem. Soc.*, 1998, **145**, 1415.

45. B. Veeraraghavan, J. Paul, B. Haran and B. Popov, *J. Power Sources*, 2002, **109**, 377.

46. M. Gaberscek, M. Bele, J. Drofenik, R. Dominko and S. Pejovnik, *J. Power Sources*, 2001, **97/98**, 67.

47. C. K. Chan, H. Peng, G. Liu, K. McIlwrath, X. F. Zhang, R. A. Huggins and Y. Cui, *Nature Nanotechnology* 2008, **3**, 31.

48. Y. D. Ko, J. G. Kang, J. G. Park, S. Lee and D. W. Kim, *Nanotechnology*, 2009, **20**, 455701.

49. Y. Li, B. Tan and Y. Wu, *J Am Chem Soc*, 2006, **128**, 14258.

50. Y. Li, B. Tan and Y. Wu, *Nano Lett.*, 2008, **8**, 265-270.

51. G. Armstrong, A. R. Armstrong, P. G. Bruce, P. Reale and B. Scrosati, *Adv Mater*, 2006, **18**, 2597.

52. F. Y. Cheng, J. Z. Zhao, W. Song, C. S. Li, H. Ma, J. Chen and P. Shen, *Inorg. Chem.*, 2006, **45**, 2038.

53. T. X. T. Sayle, R. R. Maphanga, P. E. Ngoepe and D. C. Sayle, *J Am Chem Soc*, 2009, **131**, 6161.

54. J. W. Lee, A. S. Hall, J.-D. Kim and T. E. Mallouk, *Chemistry of Materials*, 2012, **24**, 1158-1164.

55. Z. Xiao, Y. Xia, Z. Ren, Z. Liu, G. Xu, C. Chao, X. Li, G. Shena and G. Han, *J. Mater. Chem.*, 2012, **22**, 20566.

56. Z. Y. Wang, D. Y. Luan, S. Madhavi, C. M. Li and X. W. Lou, *Chem Commun*, 2011, **47**, 8061-8063.

57. C. J. Patrissi and C. R. Martin, *J. Electrochem. Soc.*, 1999, **146**, 3176-3180.

58. K. Takahashi, Y. Wang and G. Z. Cao, *J. Phys. Chem. B*, 2005, **109**, 48.

59. Y. Wang, K. Takahashi, H. M. Shang, K. H. Lee and G. Z. Cao, *J. Phys. Chem. B*, 2005, **109**, 3085.

60. Y. Wang, K. Takahashi, K. Lee and G. Z. Cao, *Adv. Funct. Mater.*, 2006, **16**, 1133.

61. K. Takahashi, Y. Wang and G. Z. Cao, *Appl. Phys. Lett.*, 2005, **86**, 053102.

62. K. Takahashi, S. J. Limmer, Y. Wang and G. Z. Cao, *Jpn. J. Appl. Phys. Part I*, 2005, **44**, 662.

63. H. B. Wu, J. S. Chen, H. H. Hng and X. W. Lou, *Nanoscale*, 2012, **4**, 2526.

64. J. Liu and D. Xue, *Nanoscale Res Lett* 2010, **5**, 1525-1534.

65. L. Su, Y. Jing and Z. Zhou, *Nanoscale*, 2011, **3**, 3967.

66. Z. Wang, D. Luan, F. Y. C. Boey and X. W. D. Lou, *J Am Chem Soc*, 2011, **133**, 4738-4741.

67. X. W. Lou, L. A. Archer and Z. Yang, *Adv Mater*, 2008, **20**, 3987-4019.

68. S. Ding, J. S. Chen, G. Qi, X. Duan, Z. Wang, E. P. Giannelis, L. A. Archer and X. W. Lou, *J Am Chem Soc*, 2011, **133**, 21-23.

69. X. W. Lou, C. Yuan and L. A. Archer, *Small*, 2007, **3**, 261.

70. B. Wang, J. S. Chen, H. B. Wu, Z. Wang and X. W. Lou, *J Am Chem Soc*, 2011, **133**, 17146–17148.

71. J. S. Chen, C. M. Li, W. W. Zhou, Q. Y. Yan, L. A. Archer and X. W. Lou, *Nanoscale*, 2009, **1**, 280-285.

72. X. Xia, J. Tu, Y. Zhang, X. Wang, C. Gu, X.-b. Zhao and H. J. Fan, *ACS Nano*, 2012, **6**, 5531-5538.

73. M.-S. Wu and H.-W. Chang, *J. Phys. Chem. C*, 2013, **117**, 2590-2599.

74. J.-Y. Liao, D. Higgins, G. Lui, V. Chabot, X. Xiao and Z. Chen, *Nano Lett.*, 2013, **13**, 5467-5473.

75. C. Chenga and H. J. Fan, *Nano Today*, 2012, **7**, 327-343.

76. J. Jiang, Y. Y. Li, J. P. Liu, X. T. Huang, C. Z. Yuan and X. W. Lou, *Adv Mater*, 2012, **24**, 5166-5180.

This journal is © The Royal Society of Chemistry 2014

*J. Mater. Chem.* A, 2014, **00**, 1-3 | **22**

77. X. W. Li, D. Li, L. Qiao, X. H. Wang, X. L. Sun, P. Wang and D. Y. He, *J Mater Chem*, 2012, **22**, 9189-9194.

78. W. Zhou, C. Cheng, J. Liu, Y. Y. Tay, J. Jiang, X. Jia, J. Zhang, H. Gong, H. H. Hng, T. Yu and H. J. Fan, *Adv. Funct. Mater.*, 2011, **21**, 2439–2445.

79. S. Zhou, X. Liu and D. Wang, *Nano Lett.*, 2010, **10**, 860-863.

80. S. Zhou, X. H. Liu, Y. J. Lin and D. W. Wang, *Angew. Chem. Int. Ed.*, 2008, **47**, 7681-7684.

81. S. Zhou, X. Liu, Y. Lin and D. Wang, *Chemistry of Materials*, 2009, **21**, 1023-1027.

82. M. Winter, J. O. Besenhard, M. E. Spahr and P. Novak, *Adv. Mater.*, 1998, **10**, 725.

83. F. B. Su, J. H. Zeng, X. Y. Bao, Y. S. Yu, J. Y. Lee and X. S. Zhao, *Chemistry of Materials*, 2005, **17**, 3960-3967.

84. K. Persson, V. A. Sethuraman, L. J. Hardwick, Y. Hinuma, Y. S. Meng, A. van der Ven, V. Srinivasan, R. Kostecki and G. Ceder, *J Phys Chem Lett*, 2010, **1**, 1176-1180.

85. Z. Yang, H. Q. Wu and B. Simard, *Electrochem Commun*, 2002, **4**, 574.

86. J. Y. Eom, H. S. Kwon, J. Liu and O. Zhou, *Carbon*, 2004, **42**, 2589.

87. J. Y. Eom, D. Y. Kim and H. S. Kwon, *J. Power Sources*, 2006, **157**, 507.

88. B. Gao, C. Bower, J. D. Lorentzen, L. Fleming, A. Kleinhammes, X. P. Tang, L. E. McNeil, Y. Wu and O. Zhou, *Chemical Physics Letters*, 2000, **327**, 69-75.

89. K. Evanoff, J. Khan, A. A. Balandin, A. Magasinski, W. J. Ready, T. F. Fuller and G. Yushin, *Adv. Mater.*, 2012, **24**, 533.

90. D. N. Futaba, K. Hata, T. Yamada, T. Hiraoka, Y. Hayamizu, Y. Kakudate, O. Tanaike, H. Hatori, M. Yumura and S. Iijima, *Nat Mater*, 2006, **5**, 987-994.

91. X. X. Wang, J. N. Wang, H. Chang and Y. F. Zhang, *Adv Funct Mater*, 2007, **17**, 3613-3618.

92. L. W. Ji, Z. Lin, M. Alcoutlabi and X. W. Zhang, *Energ Environ Sci*, 2011, **4**, 2682-2699.

93. E. Frackowiak, S. Gautier, H. Gaucher, S. Bonnamy and F. Beguin, *Carbon*, 1999, **37**, 61-69.

94. H. Xia, M. O. Lai and L. Lu, *J Mater Chem*, 2010, **20**, 6896-6902.

95. Z. H. Wen, S. Q. Ci, S. Mao, S. M. Cui, Z. He and J. H. Chen, *Nanoscale Research Letters*, 2013, **8**.

96. Y. M. Shi, Y. Wang, J. I. Wong, A. Y. S. Tan, C. L. Hsu, L. J. Li, Y. C. Lu and H. Y. Yang, *Sci Rep-Uk*, 2013, **3**, 2169.

97. K. Bindumadhavan, S. K. Srivastava and S. Mahanty, *Chem Commun*, 2013, **49**, 1823-1825.

98. Y. Nomura, I. V. Anoshkin, C. Okuda, M. Iijima, Y. Ukyo, H. Kamiya, A. G. Nasibulin and E. I. Kauppinen, *Journal of Nanoparticles*, 2014, 1-7.

99. Y. Z. Wu, M. V. Reddy, B. V. R. Chowdari and S. Ramakrishna, *Acs Appl Mater Inter*, 2013, **5**, 12175-12184.

100. L. W. Ji and X. W. Zhang, *Nanotechnology*, 2009, **20**.

101. W. Luo, J. Schardt, C. Bommier, B. Wang, J. Razink, J. Simonsen and X. L. Ji, *J Mater Chem A*, 2013, **1**, 10662-10666.

102. V. Subramanian, H. W. Zhu and B. Q. Wei, *J Phys Chem B*, 2006, **110**, 7178-7183.

103. D. Deng and J. Y. Lee, *Chemistry of Materials*, 2007, **19**, 4198-4204.

104. C. Y. Wu, X. P. Li, W. S. Li, B. Li, Y. Q. Wang, Y. T. Wang, M. Q. Xu and L. D. Xing, *Journal of Power Sources*, 2014, **251**, 85-91.

105. Y. Yu, L. Gu, C. L. Wang, A. Dhanabalan, P. A. van Aken and J. Maier, *Angew Chem Int Edit*, 2009, **48**, 6485-6489.

106. W. L. Lu, C. H. Luo, Y. Li, Y. Y. Feng, W. Feng, Y. H. Zhao and X. Y. Yuan, *J Nanopart Res*, 2013, **15**.

107. Z. X. Yang, G. D. Du, Q. Meng, Z. P. Guo, X. B. Yu, Z. X. Chen, T. L. Guo and R. Zeng, *J Mater Chem*, 2012, **22**, 5848-5854.

108. L. Ji, O. Toprakci, M. Alcoutlabi, Y. Yao, Y. Li, S. Zhang, B. Guo, Z. Lin and X. Zhang, *ACS Appl. Mater. Interfaces*, 2012, **4**, 2672–2679.

109. P. Guo, H. H. Song and X. H. Chen, *Electrochem Commun*, 2009, **11**, 1320-1324.

110. D. Pan, S. Wang, B. Zhao, M. Wu, H. Zhang, Y. Wang and Z. Jiao, *Chemistry of Materials*, 2009, **21**, 3136-3142.

111. K. S. Novoselov, A. K. Geim, S. V. Morozov, D. Jiang, Y. Zhang, S. V. Dubonos, I. V. Grigorieva and A. A. Firsov, *Science*, 2004, **306**, 666.

112. A. K. Geim and K. S. Novoselov, *Nat Mater*, 2007, **6**, 183 - 191.

113. C. Wang, D. Li, C. O. Too and G. G. Wallace, *Chemistry of Materials*, 2009, **21**, 2604–2606.

114. E. Yoo, J. Kim, E. Hosono, H. Zhou, T. Kudo and I. Honma, *Nano Lett*, 2008, **8**, 2277-2282.

115. S. L. Chou, J. Z. Wang, M. Choucair, H. K. Liu, J. A. Stride and S. X. Dou, *Electrochem Commun*, 2010, **12**, 303-306.

116. G. X. Wang, B. Wang, X. L. Wang, J. Park, S. X. Dou, H. Ahn and K. Kim, *J Mater Chem*, 2009, **19**, 8378-8384.

117. Z. S. Wu, W. C. Ren, L. Wen, L. B. Gao, J. P. Zhao, Z. P. Chen, G. M. Zhou, F. Li and H. M. Cheng, *Acs Nano*, 2010, **4**, 3187-3194.

118. C. X. Peng, B. D. Chen, Y. Qin, S. H. Yang, C. Z. Li, Y. H. Zuo, S. Y. Liu and J. H. Yang, *Acs Nano*, 2012, **6**, 1074-1081.

119. W. B. Yue, Z. Z. Lin, S. H. Jiang and X. J. Yang, *J Mater Chem*, 2012, **22**, 16318-16323.

120. D. Wang, D. Choi, J. Li, Z. Yang, Z. Nie, R. Kou, D. Hu, C. Wang, L. V. Saraf, J. Zhang, I. A. Aksay and J. Liu, *ACS Nano*, 2009, **3**, 907-914.

121. X. Xin, X. F. Zhou, J. H. Wu, X. Y. Yao and Z. P. Liu, *Acs Nano*, 2012, **6**, 11035-11043.

122. X. J. Zhu, Y. W. Zhu, S. Murali, M. D. Stollers and R. S. Ruoff, *Acs Nano*, 2011, **5**, 3333-3338.

123. B. Li, H. Cao, J. Shao and M. Qu, *Chem Commun*, 2011, **47**, 10374–10376.

124. S. K. Behera, *Chem Commun*, 2011, **47**, 10371–10373.

125. P. Lian, X. Zhu, H. Xiang, Z. Li, W. Yang and H. Wang, *Electrochim Acta*, 2010, **56**, 834–840.

126. M. Zhang, D. N. Lei, X. M. Yin, L. B. Chen, Q. H. Li, Y. G. Wang and T. H. Wang, *J Mater Chem*, 2010, **20**, 5538-5543.

127. Y. Q. Zou, J. Kan and Y. Wang, *J Phys Chem C*, 2011, **115**, 20747-20753.

128. L. Chen, Z. Y. Wang, C. N. He, N. Q. Zhao, C. S. Shi, E. Z. Liu and J. J. Li, *Acs Appl Mater Inter*, 2013, **5**, 9537-9545.

129. L. Li, A.-R. O. Raji and J. M. Tour, *Adv. Mater.*, 2013, **25**, 6298–6302.

130. H. L. Wang, L. F. Cui, Y. A. Yang, H. S. Casalongue, J. T. Robinson, Y. Y. Liang, Y. Cui and H. J. Dai, *J Am Chem Soc*, 2010, **132**, 13978-13980.

131. B. Wang, X. L. Wu, C. Y. Shu, Y. G. Guo and C. R. Wang, *J Mater Chem*, 2010, **20**, 10661-10664.

Journal of Materials Chemistry A Accepted Manuscript

132. G. M. Zhou, D. W. Wang, L. C. Yin, N. Li, F. Li and H. M. Cheng, *Acs Nano*, 2012, **6**, 3214-3223.

133. L. S. Zhang, L. Y. Jiang, H. J. Yan, W. D. Wang, W. Wang, W. G. Song, Y. G. Guo and L. J. Wan, *J Mater Chem*, 2010, **20**, 5462-5467.

134. F. Cheng, Z. Tao, J. Liang and J. Chen, *Chemistry of Materials*, 2008, **20**, 667-681.

135. H. S. Zhou, S. M. Zhu, M. Hibino, I. Honma and M. Ichihara, *Adv Mater*, 2003, **15**, 2107-2111.

136. T. Wang, X. Y. Liu, D. Y. Zhao and Z. Y. Jiang, *Chemical Physics Letters*, 2004, **389**, 327-331.

137. C. J. Meyers, S. D. Shah, S. C. Patel, R. M. Sneeringer, C. A. Bessel, N. R. Dollahon, R. A. Leising and E. S. Takeuchi, *J Phys Chem B*, 2001, **105**, 2143-2152.

138. L. O. Adam P. Cohn, Rachel Carter, Shahana Chatterjee, Andrew S. Westover, Keith Sharea, Cary L. Pint, *Nanoscale*, 2014, 4669-4675.

139. E. Ferg, R. J. Gummow, A. Dekock and M. M. Thackeray, *J. Electrochem. Soc.*, 1994, **141**, L147.

140. S. Y. Yin, L. Song, X. Y. Wang, M. F. Zhang, K. L. Zhang and Y. X. Zhang, *Electrochim Acta*, 2009, **54**, 5629.

141. D. Peramunage and K. M. Abraham, *J. Electrochem. Soc.*, 1998, **145**, 2609.

142. Y. G. Wang, Y. R. Wang, E. J. Hosono, K. X. Wang and H. S. Zhou, *Angew. Chem. Int. Ed.*, 2008, **47**, 7461.

143. Y. G. Wang, H. M. Liu, K. X. Wang, H. Eiji, Y. R. Wang and H. S. Zhou, *J. Mater. Chem.*, 2009, **19**, 6789.

144. W. J. H. Borghols, M. Wagemaker, U. Lafont, E. M. Kelder and F. M. Mulder, *J Am Chem Soc*, 2009, **131**, 17786.

145. J. L. Allen, T. R. Jow and J. Wolfenstine, *J. Power Sources*, 2006, **159**, 1340.

146. A. Jaiswal, C. R. Horne, O. Chang, W. Zhang, W. Kong, E. Wang, T. Cherm and M. M. Doeff, *J. Electrochem. Soc.*, 2009, **156**, A1041.

147. Y. Tang, L. Yang, S. Fang and Z. Qiu, *Electrochim Acta*, 2009, **54**, 6244-6249.

148. J. Y. Kim and J. P. Cho, *Electrochem. Solid-State Lett.*, 2007, **10**, A81.

149. K.-S. Park, A. Benayad, D.-J. Kang and S.-G. Doo, *J Am Chem Soc*, 2008, **130**, 14930–14931.

150. H. Li, L. Shen, J. Wang, B. Ding, P. Nie, G. Xu, X. Wang and X. Zhang, *Chem Plus Chem*, 2013, ASAP (doi: 10.1002/cplu.201300316).

151. J. Yang, M. Winter and J. O. Besenhard, *Solid State Ionics*, 1996, **90**, 281.

152. *US Patent 4,436,796 Pat.*, 1984.

153. C.-M. Park, J.-H. Kim, H. Kim and H.-J. Sohn, *Chem. Soc. Rev.*, 2010, **39**, 3115-3141.

154. M. G. Kim and J. Cho, *Adv Funct Mater*, 2009, **19**, 1497-1514.

155. M. Pharr, K. J. Zhao, X. W. Wang, Z. G. Suo and J. J. Vlassak, *Nano Lett*, 2012, **12**, 5039-5047.

156. S. W. Lee, M. T. McDowell, J. W. Choi and Y. Cui, *Nano Lett*, 2011, **11**, 3034-3039.

157. X. H. Liu, J. W. Wang, S. Huang, F. F. Fan, X. Huang, Y. Liu, S. Krylyuk, J. Yoo, S. A. Dayeh, A. V. Davydov, S. X. Mao, S. T. Picraux, S. L. Zhang, J. Li, T. Zhu and J. Y. Huang, *Nature Nanotechnology*, 2012, **7**, 749-756.

158. M. T. McDowell, I. Ryu, S. W. Lee, C. M. Wang, W. D. Nix and Y. Cui, *Adv Mater*, 2012, **24**, 6034–6041.

159. L. P. Xu, C. Kim, A. K. Shukla, A. G. Dong, T. M. Mattox, D. J. Milliron and J. Cabana, *Nano Lett*, 2013, **13**, 1800-1805.

160. B. Wang, B. Luo, X. L. Li and L. J. Zhi, *Mater Today*, 2012, **15**, 544-552.

161. C. J. Wen, B. A. Boukamp, R. A. Huggins and W. Weppner, *J. Electrochem. Soc.*, 1979, **126**, 2258.

162. Y. Liu, N. S. Hudak, D. L. Huber, S. J. Limmer, J. P. Sullivan and J. Y. Huang, *Nano Lett*, 2011, **11**, 4188-4194.

163. J. Benson, S. Boukhalfa, A. Magasinski, A. Kvit and G. Yushin, *Acs Nano*, 2012, **6**, 118-125.

164. J. Saint, M. Morcrette, D. Larcher and J. M. Tarascon, *Solid State Ionics*, 2005, **176**, 189.

165. S. Yoon, C. M. Park and H. J. Sohn, *Electrochem Solid St*, 2008, **11**, A42-A45.

166. L. Baggetto and P. H. L. Notten, *J Electrochem Soc*, 2009, **156**, A169-A175.

167. M. Martos, J. Morales and L. Sanchez, *Electrochim Acta*, 2003, **48**, 615-621.

168. A. Dailly, J. Ghanbaja, P. Willmann and D. Billaud, *Electrochim Acta*, 2003, **48**, 977.

169. J. Wang, I. D. Raistrick and R. A. Huggins, *J. Electrochem. Soc.*, 1986, **133**, 457.

170. C. J. Wen and R. A. Huggins, *J Solid State Chem*, 1981, **37**, 271.

171. P. Limthongkul, Y.-I. Jang, N. J. Dudney and Y.-M. Chiang, *Acta Mater.*, **51**, 1103.

172. Z. Wang, M. Gu, Y. Zhou, X. Zu, J. G. Connell, J. Xiao, D. Perea, L. J. Lauhon, J. Bang, S. Zhang, C. Wang and F. Gao, *Nano Lett.*, 2013, **13**, 4511.

173. T. Song, J. L. Xia, J. H. Lee, D. H. Lee, M. S. Kwon, J. M. Choi, J. Wu, S. K. Doo, H. Chang, W. Il Park, D. S. Zang, H. Kim, Y. G. Huang, K. C. Hwang, J. A. Rogers and U. Paik, *Nano Lett*, 2010, **10**, 1710-1716.

174. N. Nitta and G. Yushin, *Part Part Syst Charact* 2013, **31**, 317–336.

175. A. N. Dey, *J. Electrochem. Soc.*, 1971, **118**, 1547.

176. C. S. Fuller and J. C. Severiens, *Physical Review*, 1954, **96**, 21.

177. H. Kim, J. Choi, H.-J. Sohn and T. Kang, *J. Electrochem. Soc.*, 1999, **146**, 4401.

178. S.-M. Hwang, H.-Y. Lee, S.-W. Jang, S.-M. Lee, S.-J. Lee, H.-K. Baik and J.-Y. Lee, *Ecs Solid State Lett*, 2001, **4**, A97.

179. U. Kasavajjula, C. S. Wang and A. J. Appleby, *Journal of Power Sources*, 2007, **163**, 1003-1039.

180. M. D. Fleischauer, J. M. Topple and J. R. Dahn, *Electrochem. Solid-State Lett.*, 2005, **8**, A137.

181. Y.-L. Kim, H.-Y. Lee, S.-W. Jang, S.-H. Lim, S.-J. Lee, H.-K. Baik, Y.-S. Yoon and S.-M. Lee, *Electrochim Acta*, 2003, **48**, 2593.

182. J.-B. Kim, H.-Y. Lee, K.-S. Lee, S.-H. Lim and S.-M. Lee, *Electrochem Commun*, 2003, **5**, 544.

183. A. R. Park, J. S. Kim, K. S. Kim, K. Zhang, J. Park, J. H. Park, J. K. Lee and P. J. Yoo, *Acs Appl Mater Inter*, 2014, **6**, 1702-1708.

184. X.-L. Wang, W.-Q. Han, J. Chen and J. Graetz, *ACS Appl. Mater. Interfaces*, 2010, **2**, 1548-1551.

185. H. C. Shin and M. L. Liu, *Adv. Funct. Mater.*, 2005, **15**, 582-586.

186. R. Alcantara, U. Nwokeke, I. Rodriguez and J. L. Tirado, *Electrochem Solid St*, 2008, **11**, A209–A213.

187. J. Hassoun, S. Panero, P. Simon, P. L. Taberna and B. Scrosati, *Adv. Mater.*, 2007, **19**, 1632–1635.

**Journal of Materials Chemistry A Accepted Manuscript**

188. C. Q. Zhang, J. P. Tu, X. H. Huang, Y. F. Yuan, S. F. Wang and F. Mao, *J. Alloys Compd.*, 2008, **457**, 81-85.

189. L. Y. Beaulieu and J. R. Dahn, *J. Electrochem. Soc.*, 2000, **147**, 3237– 3241.

190. M. Z. Xue and Z. W. Fu, *Solid State Ionics*, 2006, **177**, 1501-1507.

191. K. K. D. Ehinon, S. Naille, R. Dedryvere, P. E. Lippens, J. C. Jumas and D. Gonbeau, *Chemistry of Materials*, 2008, **20**, 5388-5398.

192. H. Li, L. H. Shi, W. Lu, X. J. Huang and L. Q. Chen, *J. Electrochem. Soc.*, 2001, **148**, A915–A922.

193. Y. Wang and J. Y. Lee, *Angew. Chem. Int. Ed.*, 2006, **45**, 7039 – 7042.

194. J.-U. Seo and C.-M. Park, *J. Mater. Chem. A*, 2013, **1**, 15316.

195. X. Y. Wang, Z. Y. Wen, B. Lin, J. Lin, X. W. Wu and X. G. Xu, *J. Power Sources*, 2008, **184**, 508-512.

196. D. Larcher, A. S. Prakash, J. Saint, M. Morcrette and J. M. Tarascon, *Chemistry of Materials*, 2004, **16**, 5502-5511.

197. J. M. Mosby and A. L. Prieto, *J Am Chem Soc*, 2008, **130**, 10656-10661.

198. J. X. Zhu, T. Sun, J. S. Chen, W. H. Shi, X. J. Zhang, X. W. Lou, S. Mhaisalkar, H. H. Hng, F. Boey, J. Ma and Q. Y. Yan, *Chemistry of Materials*, 2010, **22**, 5333-5339.

199. S. Saadat, Y. Y. Tay, J. X. Zhu, P. F. Teh, S. Maleksaeedi, M. M. Shahjamali, M. Shakerzadeh, M. Srinivasan, B. Y. Tay, H. H. Hng, J. Ma and Q. Y. Yan, *Chemistry of Materials*, 2011, **23**, 1032-1038.

200. H. Lee and J. Cho, *Nano Lett.*, 2007, **7**, 2638-2641.

201. Y. Kwon and J. Cho, *Chem Commun*, 2008, 1109-1111.

202. O. Mao, R. L. Turner, I. A. Courtney, B. D. Fredericksen, M. I. Buckett, L. J. Krause and J. R. Dahn, *Electrochem Solid St*, 1999, **2**, 3-5.

203. C. M. Park and H. J. Sohn, *Adv Mater*, 2010, **22**, 47-52.

204. H. Jung, M. Park, Y.-G. Yoon, G.-B. Kim and S.-K. Joo, *J. Power Sources*, 2003, **115**, 346-351.

205. J. O. Besenhard, J. Yang and M. Winter, *J. Power Sources*, 1997, **68**, 87.

206. J. R. Szczech and S. Jin, *Energy Environ. Sci.*, 2011, **4**, 56.

207. H. Kim, E.-J. Lee and Y.-K. Sun, *Mater Today*, 2014, (DOI: 10.1016/j.mattod.2014.1005.1003).

208. X. Su, Q. Wu, J. Li, X. Xiao, A. Lott, W. Lu, B. W. Sheldon and J. Wu, *Adv Energy Mater*, 2014, **4**, 1300882.

209. H. Li, X. Huang, L. Chen, Z. Wu and Y. Liang, *Electrochem. Solid-State Lett.*, 1999, **2**, 547-549.

210. D. Mazouzi, B. Lestriez, L. Roue and D. Guyomard, *Electrochem. Solid-State Lett.*, 2009, **12**, A215-A218.

211. H. Kim, M. Seo, M.-H. Park and J. Cho, *Angew. Chem. Int. Ed.*, 2010, **49**, 2146.

212. M. L. Terranova, S. Orlanducci, E. Tamburri, V. Guglielmotti and M. Rossi, *J. Power Sources*, 2014, **246**, 167-177.

213. D. Shao, D. Tang, Y. Mai and L. Zhang, *J. Mater. Chem. A*, 2013, **1**, 15068.

214. P. P. Prosini, C. Cento, F. Alessandrini, P. Gislon, A. Mancini, A. Rufoloni, F. Rondino and A. Santoni, *Solid State Ionics*, 2014, **260**, 49-54.

215. L.-F. Cui, R. Ruffo, C. K. Chan, H. Peng and Y. Cui, *Nano Lett.*, 2009, **9**, 491.

216. H. Wu, G. Chan, J. W. Choi, I. Ryu, Y. Yao, M. T. McDowell, S. W. Lee, A. Jackson, Y. Yang, L. Hu and Y. Cui, *Nature Nanotechnology*, 2012, **7**, 310-315.

217. K. J. Koski and Y. Cui, *ACS Nano*, 2013, **7**, 3739-3743.

218. F.-F. Cao, J.-W. Deng, S. Xin, H.-X. Ji, O. G. Schmidt, L.-J. Wan and Y.-G. Guo, *Adv. Mater.* , 2011, **23**, 4415–4420.

219. S. Zhou and D. W. Wang, *Acs Nano*, 2010, **4**, 7014-7020.

220. X. Fan, H. Zhang, N. Du, P. Wu, X. Xu, Y. Li and D. Yang, *Nanoscale*, 2012, **4**, 5343-5347.

221. P. R. Abel, A. M. Chockla, Y.-M. Lin, V. C. Holmberg, J. T. Harris, B. A. Korgel, A. Heller and C. B. Mullins, *ACS Nano*, 2013, **7**, 2249-2257.

222. J. A. Jiang, Y. Y. Li, J. P. Liu and X. T. Huang, *Nanoscale*, 2011, **3**, 45-58.

223. Y. Idota, T. Kubota, A. Matsufuji, Y. Maekawa and T. Miyasaka, *Science*, 1997, **276**, 1395-1397.

224. J. S. Chen and X. W. Lou, *Small*, 2013, **9**, 1877-1893.

225. D. Larcher, S. Beattie, M. Morcrette, K. Edstrom, J.-C. Jumas and J.-M. Tarascon, *J. Mater. Chem.*, 2007, **17**, 3759.

226. R. Demir-Cakan, Y. S. Hu, M. Antonietti, J. Maier and M. M. Titirici, *Chemistry of Materials*, 2008, **20**, 1227-1229.

227. X. W. Lou, Y. Wang, C. Yuan, J. Y. Lee and L. A. Archer, *Adv Mater*, 2006, **18**, 2325-2329.

228. P. Meduri, C. Pendyala, V. Kumar, G. U. Sumanasekera and M. K. Sunkara, *Nano Lett*, 2009, **9**, 612-616.

229. J. P. Liu, Y. Y. Li, X. T. Huang, R. M. Ding, Y. Y. Hu, J. Jiang and L. Liao, *J Mater Chem*, 2009, **19**, 1859-1864.

230. P. Roy, S. Berger and P. Schmuki, *Angew. Chem. Int. Ed.*, 2011, **50**, 2904-2939.

231. P. Roy, D. Kim, K. Lee, E. Spiecker and P. Schmuki, *Nanoscale*, 2010, **2**, 45-59.

232. P. Roy, C. Das, K. Lee, R. Hahn, T. Ruff, M. Moll and P. Schmuki, *J Am Chem Soc*, 2011, **133**, 5629-5631.

233. Z. G. Yang, D. Choi, S. Kerisit, K. M. Rosso, D. H. Wang, J. Zhang, G. Graff and J. Liu, *J. Power Sources*, 2009, **192**, 588.

234. J. S. Chen, Y. L. Tan, C. M. Li, Y. L. Cheah, D. Luan, S. Madhavi, F. Y. C. Boey, L. A. Archer and X. W. Lou, *J Am Chem Soc*, 2010, **132**, 6124-6130.

235. H. G. Yang, C. H. Sun, S. Z. Qiao, J. Zou, G. Liu, S. C. Smith, H. M. Cheng and G. Q. Lu, *Nature*, 2008, **453**, 638-641.

236. C. H. Sun, X. H. Yang, J. S. Chen, Z. Li, X. W. Lou, C. Li, S. C. Smith, G. Q. M. Luc and H. G. Yang, *Chem Commun*, 2010, **46**, 6129-6131.

237. J.-G. Kim, D. Shi, K.-J. Kong, Y.-U. Heo, J. H. Kim, M. R. Jo, Y. C. Lee, Y.-M. Kang and S. X. Dou, *ACS Appl. Mater. Interfaces*, 2013, **5**, 691-696.

238. C. Zhu, X. Xia, J. Liu, Z. Fan, D. Chao, H. Zhang and H. J. Fan, *Nano Energy*, 2014, **4**, 105-112.

239. J.-H. Jeun, K.-Y. Park, D.-H. Kim, W.-S. Kim, H.-C. Kim, B.-S. Lee, H. Kim, W.-R. Yu, K. Kang and S.-H. Hong, *Nanoscale*, 2013, **5**, 8480.

240. G. Ji, B. Ding, Y. Ma and J. Y. Lee, *Environ Technol*, 2013, **1**, 567.

241. X. Wu, S. Zhang, L. Wang, Z. Du, H. Fang, Y. Ling and Z. Huang, *J. Mater. Chem.*, 2012, **22**, 11151.

242. W. Wang, Q. Sa, J. Chen, Y. Wang, H. Jung and Y. Yin, *ACS Appl. Mater. Interfaces*, 2013, **5**, 6478.

This journal is © The Royal Society of Chemistry 2014

*J. Mater. Chem*. A, 2014, **00**, 1-3 | **25**

243. F. F. Cao, Y. G. Guo, S. F. Zheng, X. L. Wu, L. Y. Jiang, R. R. Bi, L. J. Wan and J. Maier, *Chemistry of Materials*, 2010, **22**, 1908-1914.

244. H. Lai, J. Li, Z. Chen and Z. Huang, *ACS Appl. Mater. Interfaces*, 2012, **4**, 2325.

245. D. Larcher, C. Masquelier, D. Bonnin, Y. Chabre, V. Masson, J.-B. Leriche and J.-M. Tarascon, *J. Electrochem. Soc.*, 2003, **150**, A133-A139.

246. D. Larcher, D. Bonnin, R. Cortes, I. Rivals, L. Personnaz and J.-M. Tarascon, *J. Electrochem. Soc.*, 2003, **150**, A1643-A1650.

247. M. V. Reddy, T. Yu, C.-H. Sow, Z. X. Shen, C. T. Lim, G. V. S. Rao and B. V. R. Chowdari, *Adv. Funct. Mater.*, 2007, **17**, 2792-2799.

248. Y. Q. Song, S. S. Qin, Y. W. Zhang, W. Q. Gao and J. P. Liu, *J Phys Chem C*, 2010, **114**, 21158-21164.

249. J. P. Liu, Y. Y. Li, H. J. Fan, Z. H. Zhu, J. Jiang, R. M. Ding, Y. Y. Hu and X. T. Huang, *Chemistry of Materials*, 2010, **22**, 212-217.

250. J. Chen, L. Xu, W. Li and X. Gou, *Adv. Mater.*, 2005, **17**, 582.

251. J. S. Chen, T. Zhu, X. H. Yang, H. G. Yang and X. W. Lou, *J Am Chem Soc*, 2010, **132**, 13162-13164.

252. B. Koo, H. Xiong, M. D. Slater, V. B. Prakapenka, M. Balasubramanian, P. Podsiadlo, C. S. Johnson, T. Rajh and E. V. Shevchenko, *Nano Lett.*, 2012, **12**, 2429-2435.

253. S. Liu, L. Zhang, J. Zhou, J. Xiang, J. Sun and J. Guan, *Chemistry of Materials*, 2008, **20**, 3623-3628.

254. W. W. Zhou, Y. Y. Tay, X. T. Jia, D. Y. Y. Wai, J. Jiang, H. H. Hng and T. Yu, *Nanoscale*, 2012, **4**, 4459-4463.

255. H. Wu, M. Xu, Y. C. Wang and G. F. Zheng, *Nano Res*, 2013, **6**, 167-173.

256. J. Morales, L. Sánchez, F. Martín, F. Berry and X. Ren, *J. Electrochem. Soc.*, 2005, **152**, A1748.

257. H. El-Shinawi, A. S. Schulze, M. Neumeier, T. Leichtweiß and J. r. Janek, *J. Phys. Chem. C*, 2014, **118**, 8818-8823.

258. L. Taberna, S. Mitra, P. Poizot, P. Simon and J. M. Tarascon, *Nat Mater*, 2006, **5**, 567.

259. L. Shen, H. Song, H. Cui, X. Wen, X. Wei and C. Wang, *Cryst Eng Comm*, 2013, **15**, 9849-9854.

260. C. He, S. Wu, N. Zhao, C. Shi, E. Liu and J. Li, *ACS Nano*, 2013, **7**, 4459–4469.

261. Z. P. Zeng, H. L. Zhao, J. Wang, P. P. Lv, T. H. Zhang and Q. Xia, *Journal of Power Sources*, 2014, **248**, 15-21.

262. T. Zhu, J. S. Chen and X. W. D. Lou, *J. Phys. Chem. C*, 2011, **115**, 9814-9820.

263. T. Muraliganth, A. V. Murugan and A. Manthiram, *Chem Commun*, 2009, 7360.

264. L. M. Lang and Z. Xu, *Acs Appl Mater Inter*, 2013, **5**, 1698-1703.

265. J. Wang, L. Li, C. L. Wong, L. Sun, Z. Shen and S. Madhavi, *Rsc Adv*, 2013, **3**, 15316.

266. R. Li, X. Ren, F. Zhang, C. Du and J. Liu, *Chem Commun*, 2012, **48**, 5010-5012.

267. P. Poizot, S. Laruelle, S. Grugeon, L. Dupont and J. M. Tarascon, *Nature*, 2000, **407**, 496.

268. G. Binotto, D. Larcher, A. S. Prakash, R. H. Urbina, M. S. Hegde and J. M. Tarascon, *Chemistry of Materials*, 2007, **19**, 3032-3040.

269. Y. Qi, H. Zhang, N. Du, C. X. Zhai and D. R. Yang, *Rsc Adv*, 2012, **2**, 9511-9516.

270. W. Y. Li, L. N. Xu and J. Chen, *Adv Funct Mater*, 2005, **15**, 851-857.

271. M. Y. Son, Y. J. Hong and Y. C. Kang, *Chem Commun*, 2013, **49**, 5678-5680.

272. J. Wang, N. Yang, H. Tang, Z. Dong, Q. Jin, M. Yang, D. Kisailus, H. Zhao, Z. Tang and D. Wang, *Angew. Chem. Int. Ed.*, 2013, **52**, 6417-6420.

273. G. Huang, S. Xu, S. Lu, L. Li and H. Sun, *ACS Appl. Mater. Interfaces*, 2014, **6**, 7236.

274. X. W. Lou, D. Deng, J. Y. Lee, J. Feng and L. A. Archer, *Adv. Mater.*, 2008, **20**, 258.

275. J. Jiang, J. P. Liu, R. M. Ding, X. X. Ji, Y. Y. Hu, X. Li, A. Z. Hu, F. Wu, Z. H. Zhu and X. T. Huang, *J Phys Chem C*, 2010, **114**, 929-932.

276. M. Zhang, E. Uchaker, S. Hu, Q. Zhang, T. Wang, G. Cao and J. Li, *Nanoscale*, 2013, **5**, 12342-12349.

277. M. X. Li, Y. X. Yin, C. J. Li, F. Z. Zhang, L. J. Wan, S. L. Xu and D. G. Evans, *Chem Commun*, 2012, **48**, 410-412.

278. L. L. Xing, Y. Y. Zhao, J. Zhao, Y. X. Nie, P. Deng, Q. Wang and X. Y. Xue, *J Alloy Compd*, 2014, **586**, 28-33.

279. J. M. Ma, J. Q. Yang, L. F. Jiao, Y. H. Mao, T. H. Wang, X. C. Duan, J. B. Lian and W. J. Zheng, *Crystengcomm*, 2012, **14**, 453-459.

280. S. Ci, J. Zou, G. Zeng, Q. Peng, S. Luo and Z. Wen, *Rsc Adv*, 2012, **2**, 5185–5192.

281. C. M. Zhang, J. Chen, Y. Zeng, X. H. Rui, J. X. Zhu, W. Y. Zhang, C. Xu, T. M. Lim, H. H. Hng and Q. Y. Yan, *Nanoscale*, 2012, **4**, 3718-3724.

282. M. Sasidharan, N. Gunawardhana, C. Senthil and a. M. Yoshio, *J. Mater. Chem. A*, 2014, **2**, 7337.

283. Y. Yu, L. Gu, C. Zhu, S. Tsukimoto, P. A. v. Aken and J. Maier, *Adv. Mater.*, 2010, **22**, 2247.

284. W. Wen, J. M. Wu and M. H. Cao, *J Mater Chem A*, 2013, **1**, 3881-3885.

285. B. Varghese, M. V. Reddy, Z. Yanwu, C. S. Lit, T. C. Hoong, G. V. S. Rao, B. V. R. Chowdari, A. T. S. Wee, C. T. Lim and C. H. Sow, *Chemistry of Materials*, 2008, **20**, 3360-3367.

286. E. Hosono, S. Fujihara, I. Honma and H. S. Zhou, *Electrochem Commun*, 2006, **8**, 284-288.

287. M.-C. Liu, L.-B. Kong, C. Lu, X.-M. Li, Y.-C. Luo and L. Kang, *ACS Appl. Mater. Interfaces*, 2012, **4**, 4631–4636.

288. S. H. Choi, J. H. Lee and Y. C. Kang, *Nanoscale*, 2013, **5**, 12645-12650.

289. J. P. Liu, Y. Y. Li, R. M. Ding, J. Jiang, Y. Y. Hu, X. X. Ji, Q. B. Chi, Z. H. Zhu and X. T. Huang, *J Phys Chem C*, 2009, **113**, 5336-5339.

290. Y. J. Feng, R. Q. Zou, D. G. Xia, L. L. Liu and X. D. Wang, *J Mater Chem A*, 2013, **1**, 9654-9658.

291. M. Ahmad, Y. Y. Shi, A. Nisar, H. Y. Sun, W. C. Shen, M. Wei and J. Zhu, *J Mater Chem*, 2011, **21**, 7723-7729.

292. Y. Cao, L. Zhang, D. Tao, D. Huo and K. Su, *Electrochim Acta*, 2014, **132**, 483-489.

293. I. Shakir, *Electrochim Acta*, 2014, **132**, 490-495.

294. F. Zheng, D. Zhu and Q. Chen, *ACS Appl. Mater. Interfaces*, 2014, **(DOI: dx.doi.org/10.1021/am501512j)**.

295. L. L. Li, S. J. Peng, Y. L. Cheah, P. F. Teh, J. Wang, G. Wee, Y. W. Ko, C. L. Wong and M. Srinivasan, *Chem-Eur J*, 2013, **19**, 5892-5898.

This journal is © The Royal Society of Chemistry 2014

*J. Mater. Chem.* A, 2014, **00**, 1-3 | **26**

296. L. Yin, Z. Zhang, Z. Li, F. Hao, Q. Li, C. Wang, R. Fan and Y. Qi, *Adv. Funct. Mater.*, 2014, **(DOI: 10.1002/adfm.201400108)**.

297. R. Wu, X. Qian, K. Zhou, J. Wei, J. Lou and P. M. Ajayan, *ACS Nano*, 2014, **(DOI:10.1021/nn501783n)**.

298. B. Liu, J. Zhang, X. Wang, G. Chen, D. Chen, C. Zhou and G. Shen, *Nano Lett.*, 2012, **12**, 3005-3011.

299. G. Huang, F. F. Zhang, L. L. Zhang, X. C. Du, J. W. Wang and L. M. Wang, *J Mater Chem A*, 2014, **2**, 8048-8053.

300. B. G. Silbernagel, *Solid State Communications*, 1975, **17**, 361-365.

301. S. K. Das, R. Mallavajula, N. Jayaprakash and L. A. Archer, *J Mater Chem*, 2012, **22**, 12988-12992.

302. U. K. Sen and S. Mitra, *Acs Appl Mater Inter*, 2013, **5**, 1240-1247.

303. K. Zhang, H. J. Kim, X. J. Shi, J. T. Lee, J. M. Choi, M. S. Song and J. H. Park, *Inorg Chem*, 2013, **52**, 9807-9812.

304. J. Xiao, D. W. Choi, L. Cosimbescu, P. Koech, J. Liu and J. P. Lemmon, *Chemistry of Materials*, 2010, **22**, 4522-4524.

305. M. Wang, G. D. Li, H. Y. Xu, Y. T. Qian and J. Yang, *Acs Appl Mater Inter*, 2013, **5**, 1003-1008.

306. C. Q. Feng, L. F. Huang, Z. P. Guo and H. K. Liu, *Electrochem Commun*, 2007, **9**, 119-122.

307. G. X. Wang, S. Bewlay, J. Yao, H. K. Liu and S. X. Dou, *Electrochem Solid St*, 2004, **7**, A321-A323.

308. H. Liu, D. W. Su, G. X. Wang and S. Z. Qiao, *J Mater Chem*, 2012, **22**, 17437-17440.

309. X. P. Fang, C. X. Hua, C. R. Wu, X. F. Wang, L. Y. Shen, Q. Y. Kong, J. Z. Wang, Y. S. Hu, Z. X. Wang and L. Q. Chen, *Chem-Eur J*, 2013, **19**, 5694-5700.

310. Y. Liu, W. Wang, H. Huang, L. Gu, Y. Wang and X. Peng, *Chem Commun*, 2014, **50**, 4485-4488.

311. K. Shiva, H. S. S. R. Matte, H. B. Rajendra, A. J. Bhattacharyya and C. N. R. Rao, *Nano Energy*, 2013, **2**, 787-793.

312. B. Kartick, S. K. Srivastava and S. Mahanty, *J Nanosci Nanotechnol*, 2014, **14**, 3758-3764.

313. J. Choi, J. Jin, I. G. Jung, J. M. Kim, H. J. Kim and S. U. Son, *Chem Commun*, 2011, **47**, 5241-5243.

314. J. T. Jang, S. Jeong, J. W. Seo, M. C. Kim, E. Sim, Y. Oh, S. Nam, B. Park and J. Cheon, *J Am Chem Soc*, 2011, **133**, 7636-7639.

315. B. Kartick, S. K. Srivastava and S. Mahanty, *J Nanopart Res*, 2013, **15**, 1950.

316. J. Chen, Z. L. Tho and S. L. Li, *Angew Chem Int Edit*, 2003, **42**, 2147-2151.

317. Z. L. Tao, L. N. Xu, X. L. Gou, J. Chen and H. T. Yuan, *Chem Commun*, 2004, 2080-2081.

318. M. S. Whittingham, *Prog. Solid State Chem.*, 1978, **12**, 41.

319. J. X. Song, M. J. Zhou, R. Yi, T. Xu, M. L. Gordin, D. H. Tang, Z. X. Yu, M. Regula and D. H. Wang, *Adv Funct Mater*, 2014, **24**, 5904-5910.

320. M. Gu, X. C. Xiao, G. Liu, S. Thevuthasan, D. R. Baer, J. G. Zhang, J. Liu, N. D. Browning and C. M. Wang, *Sci Rep-Uk*, 2014, **4**.

321. C. Erk, T. Brezesinski, H. Sommer, R. Schneider and J. Janek, *Acs Appl Mater Inter*, 2013, **5**, 7299-7307.

322. M. Armand, S. Grugeon, H. Vezin, S. Laruelle, P. Ribiere, P. Poizot and J. M. Tarascon, *Nat Mater*, 2009, **8**, 120-125.

323. A. L. M. Reddy, S. Nagarajan, P. Chumyim, S. R. Gowda, P. Pradhan, S. R. Jadhav, M. Dubey, G. John and P. M. Ajayan, *Sci Rep-Uk*, 2012, **2**.

324. M. Kaempgen, C. K. Chan, J. Ma, Y. Cui and G. Gruner, *Nano Lett*, 2009, **9**, 1872-1876.

325. K. Wang, P. Zhao, X. M. Zhou, H. P. Wu and Z. X. Wei, *J Mater Chem*, 2011, **21**, 16373-16378.

326. G. Y. Zheng, L. B. Hu, H. Wu, X. Xie and Y. Cui, *Energ Environ Sci*, 2011, **4**, 3368-3373.

327. J. F. Zang, C. Y. Cao, Y. Y. Feng, J. Liu and X. H. Zhao, *Sci Rep-Uk*, 2014, **4**.

328. L. B. Hu, H. Wu, F. La Mantia, Y. A. Yang and Y. Cui, *Acs Nano*, 2010, **4**, 5843-5848.

329. L. B. Hu, M. Pasta, F. La Mantia, L. F. Cui, S. Jeong, H. D. Deshazer, J. W. Choi, S. M. Han and Y. Cui, *Nano Lett*, 2010, **10**, 708-714.

This journal is © The Royal Society of Chemistry 2014

*J. Mater. Chem.* A, 2014, **00**, 1-3 | **27**